

Did the Variscan relief influence the Permian climate of Mesoeurope? Insights from geochemical and mineralogical proxies from Sardinia (Italy)



Rosa Sinisi ^{a,*}, Giovanni Mongelli ^b, Paola Mameli ^a, Giacomo Oggiano ^a

^a Department of Nature and Land Sciences, University of Sassari, via Piandanna 4, 07100 Sassari, Italy

^b Department of Sciences, University of Basilicata, via Ateneo Lucano 10, 85100 Potenza, Italy

ARTICLE INFO

Article history:

Received 10 September 2013

Received in revised form 3 December 2013

Accepted 19 December 2013

Available online 7 January 2014

Keywords:

Permian–Triassic red beds

Variscan relief

Palaeoclimate proxies

Sedimentary recycling

Diagenetic K-metasomatism

ABSTRACT

Red beds deposits of Permian–Triassic basins of Sardinia (western Italy), where a wide segment of the Variscan orogen is exposed, were studied. The basins were selected according to their position within the structural zones of Variscan orogen, i.e. from the external to the inner sectors of the chain. Detailed mineralogical, petrographical, and chemical analyses were performed on shale and calcrete layers laying along the sedimentary sequences, to examine their compositional features and stratigraphic variation. In this regard, enrichment factors ($F_{(e)}$) for major and trace elements (relative to the PAAS composition) were calculated and discussed. Several geochemical proxies were also calculated and used to assess the palaeoclimate conditions during the red beds deposition. The weathering indices (CIA and CIW) accounted for more humid conditions in the basins of the axial zone relative to the basins those of the foreland, which instead were characterised by an arid climate. However, the presence of carbonates, albeit discontinuous, and the values of calcification, salinity, and hydrolysis indices suggest that, in the axial zone, dry and hot periods also occurred. Compositional data of the sedimentary records were correlated to the Sardinia geological setting and significant information were obtained on the palaeoenvironment characterizing the south-western Mesoeurope during Permian and Triassic. Al_2O_3 – TiO_2 –Zr ternary plot and Zr/Sc vs. Th/Sc diagram show that both sorting and sedimentary recycling affected the studied basins. Precisely, our data lead us to suppose that a wide regional subsidence caused both the recycling of uplifted Variscan rocks and the diagenetic K-metasomatism of Permian sediments revealed by the A–CN–K diagram. Finally, a supply from upper continental source has been suggested by the provenance proxies (such as $(Gd/Yb)_N$ and Eu/Eu^*) and the La–Th–Sc plot that also reflect the paucity of mafic rocks in feeding areas.

© 2013 Elsevier B.V. All rights reserved.

1. Introduction

The interval between the early Permian and Early Triassic was a period of significant environmental change and lithospheric activity that triggered a sequence of palaeogeographical changes affecting most of the planet (López-Gómez et al., 2005; Shen, 2013). With respect to the Permian–Triassic Pangaeian regime, many factors have been proposed to account for regional and global climatic changes towards wetter as well as drier conditions. Global factors include alternating periods of greenhouse conditions (Roy and Roser, 2013) resulting from spikes in CO_2 and CH_4 , related to oxidation and/or thermogenic cracking of coal-rich Carboniferous–Permian deposits (Retallack, 2013) and eruption of basalt in the Siberian Traps (Chen et al., 2013). In the Mesoeuropean sector of Pangaea, local factors include the final Tethys opening and the Zechstein transgression, which are thought to have made the climate wetter (van Wees et al., 2000), whereas the China–Siberia collision, the onset of cool streams along the Palaeotethys

and the hindering of moisture transport from this ocean are considered to have been responsible for a drier climate (Isozaki et al., 2011; Kossovaya, 2009). Only a few authors (e.g., Fluteau et al., 2001) have argued that the relief of the Variscan Chain had a significant effect on the regional climate of this sector of Pangaea, in contrast to others (e.g., Roscher and Schneider, 2006) who claim that the chain provided a negligible east–west orographic barrier across Mesoeurope.

The Mesoeuropean crust, which after the early Permian Pangaea amalgamation was located in the western Mediterranean area, became part of a dextral strike-slip tectonic setting as the African and Eurasian plates moved apart. Throughout the Permian, several intracratonic basins developed under tensile to transtensive stress, and were filled with clastic and volcanic successions (Brouin et al., 1994; Bertoluzza and Perotti, 1997; Cortesogno et al., 1998; Zeh et al., 2000).

Subsequently, sedimentation of grey (mainly lacustrine) deposits of the Autunian facies gave way to the deposition of red beds consisting of reddish alluvial conglomerates, sandstones, and shales that are ascribed to a generic Permian–Triassic age. Most of the Permian–Triassic sedimentary sequences of southwestern Europe are characterised by a lack of paleontological evidence, making it very difficult to assign an

* Corresponding author. Tel.: +39 0971 206181.

E-mail address: rsinisi@uniss.it (R. Sinisi).

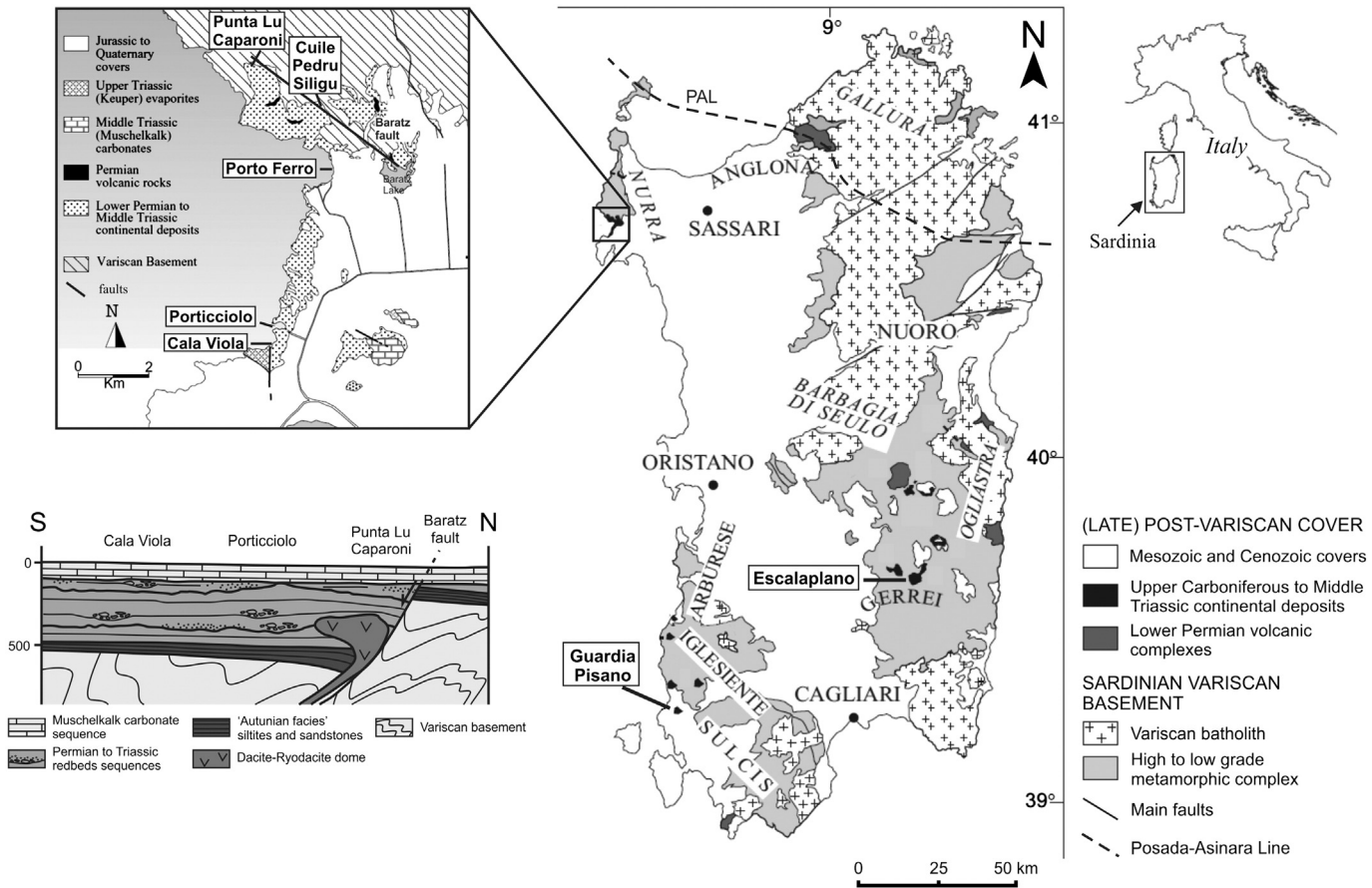


Fig. 1. Geological sketch map of Sardinia and sampling sites. The Nurra district is expanded in the box at left of figure, where a simplified geological cross section of Nurra is also shown.

age to these sediments with any certainty (Diez et al., 2005). In addition, a widespread sedimentary hiatus is recorded in the sequences of some basins, at or near the Permian–Triassic boundary, thereby limiting our ability to infer palaeoclimate and palaeoenvironmental changes during that time (De la Horra et al., 2008).

Several studies have examined the sedimentary records of southwestern European basins of Permian and Permian–Triassic age, identifying their main stratigraphic and sedimentological changes (Durand, 2008; Linol et al., 2009; López-Gómez et al., 2012). However, although good sedimentological and palaeontological data related to the sediments filling these basins have been produced, it was given scarce importance to their mineralogical and geochemical features.

The chemical composition of sedimentary rocks constitutes an important record of the geological evolution of the continental crust through time, because some elements are preferentially transferred and transported in the terrigenous clastic fraction depending on the intensity of weathering (Taylor and McLennan, 1985). Previous studies based on mineralogical and geochemical analyses of sedimentary deposits have been able to constrain the provenance of the clastic supply, to evaluate the processes determining their origin, and to infer the tectonic setting and sedimentary evolution of continental basins (e.g., Lindgreen and Surlyk, 2000; Perri et al., 2012 and references therein). In this regard, special attention has been paid to red beds, palaeosols (Sheldon and Tabor, 2009), and carbonate concretions (such as calcretes and/or dolocretes and rhizolites) because these are important indicators of the palaeoenvironmental and palaeoclimatic conditions controlling the evolution of sedimentary basins. Red beds are usually interpreted as sediments related to the weathering and erosion of structural highs bordering extensional basins under warm tropical climates with frequent arid episodes, although

some recent studies have questioned this genesis (e.g., Sheldon, 2005). Palaeosols, by definition, are located in situ and can therefore be considered as indirect evidence of relative tectonic stability and/or a low sedimentation rate (De la Horra et al., 2008). Pedogenic carbonates are limited to those climatic conditions that are sufficiently arid to allow the accumulation of alkali earth carbonates within the soil horizon (Alonso-Zarza et al., 2009), and have accordingly been used to detect very dry climate and intense evapotranspiration conditions. In Sardinia (western Mediterranean), thick Permian and Triassic sedimentary sequences occur, which have recently been compared with and correlated to similar deposits in the distal part of the Provence Trough in southeastern France (Cassinis et al., 2003). This record consists of alluvial red beds, mainly braided fluvial systems, characterised by several pedogenic layers and a carbonate horizon that commonly break up the sedimentary suite.

In this paper, which represents the first phase of a more comprehensive research project, we present the first detailed mineralogical and geochemical studies of siliciclastic deposits, palaeosols, and pedogenic (carbonate) concretions of northern and southern Sardinia, with the aim of contributing to the description and understanding of the evolution of palaeoclimate and palaeoenvironment within a part of Mesoeurope during the early–middle Permian to Early Triassic.

2. Geological and stratigraphic setting

The actual positioning of the Sardinia–Corsica Microplate is a consequence of a rotation resulting from Miocene back-arc spreading that generated the Liguro–Provençal Basin. After restoring its original pre-Burdigalian position, Sardinia was part of the Mesoeuropean crust formed during the Variscan Orogeny. The southern branch of the

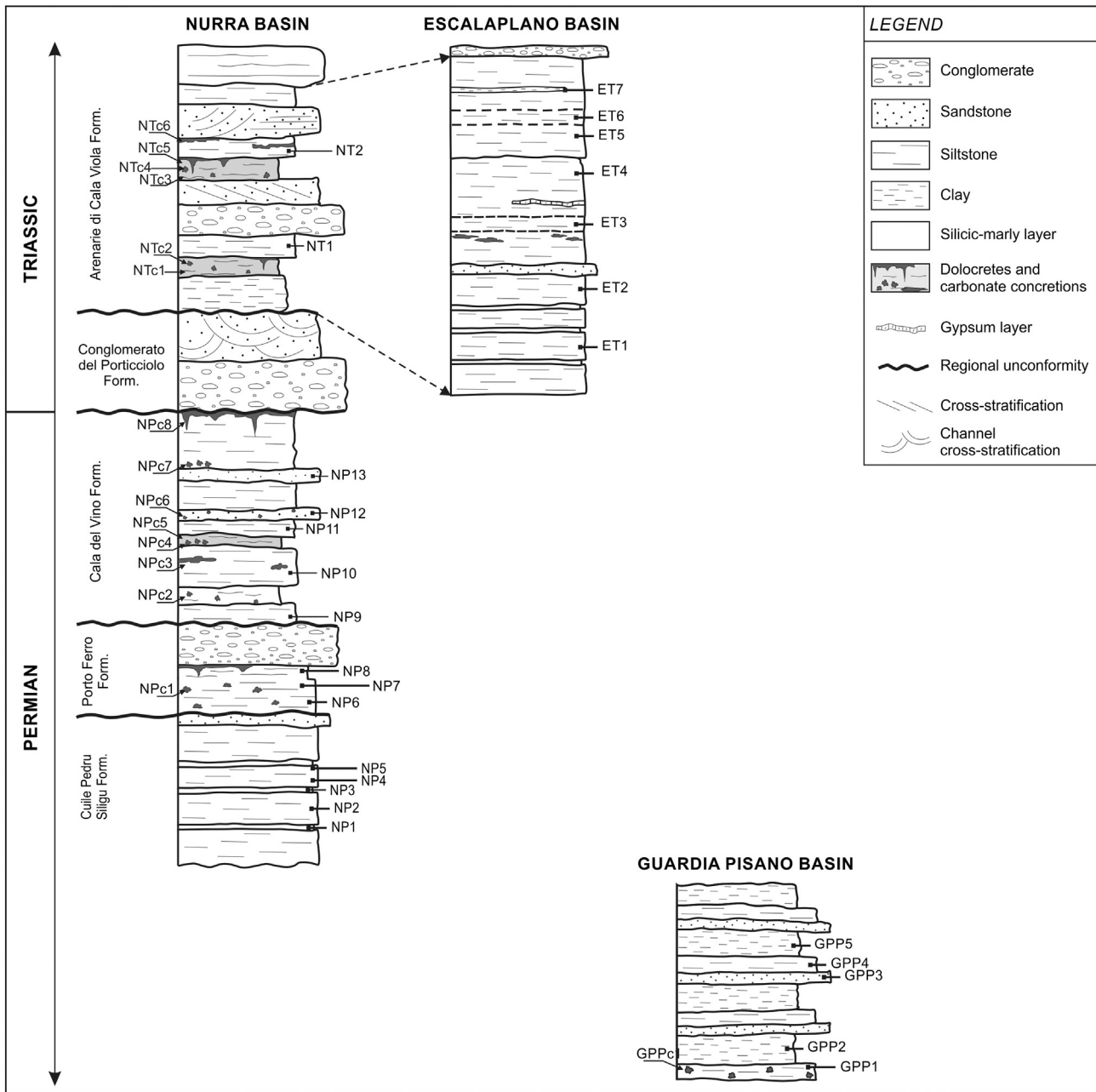


Fig. 2. Chrono-stratigraphic scheme illustrating the sedimentary successions of Nurra, Escalaplano, and Guardia Pisano basins. The stratigraphic position and the name of each sample is also shown. Not in scale.

Variscan Chain is regarded as having formed as a result of rifting, oceanic spreading, and convergence followed by continental collision (von Raumer et al., 2003). This process lasted from the Ordovician until the Dinantian and generated a thick orogenic belt (Oggiano et al., 2010).

In Sardinia a segment of the Variscan collisional belt is well exposed from south to north (Rossi et al., 2009). According to Carmignani et al. (1994), it comprises the following sections: the foreland (consisting of the southwestern part of the island), that is composed of carbonate and terrigenous successions embracing the entire Palaeozoic basement; the nappe zone (corresponding to the central part of the island), that contains a stack of nappes metamorphosed under greenschist conditions; the axial zone (ie the areas close to the Variscan relief), where were exhumed lower-mid crustal, high-grade metamorphic rocks, bearing eclogite pods similar to those of the inner crystalline nappe of the French Massif Central (Cortesogno et al., 2004; Franceschelli et al., 2007; Cruciani et al., 2010).

After the collisional evolution, a dextral strike-slip, transtensional regime was established coevally with both the emplacement of the early plutonic units and the development of several intramontane Carboniferous–Permian basins (Conti et al., 1999; Casini and Oggiano, 2008; Casini et al., 2012).

Small intramontane basins, filled with clastic and volcanic successions ranging from the upper Carboniferous to lower Triassic, are ubiquitous from the foreland to the axial zone. Among these, some basins developed close to the transtensional strike-slip shear zone, (i.e. the Posada-Asinara Line in the axial zone, Fig. 1), few basins are half graben bounded by growth faults (Buzzi et al., 2008), others are basins formed within wide late collisional synforms close to the thrusts reactivated as low-angle normal faults (in the nappe zone and foreland). Several Carboniferous and Permian–Triassic basins of Sardinia were buried by Mesozoic and/or Cainozoic sediments or else were intruded by late Variscan granitoids and experienced the thermometamorphism.

Table 1
Percentages of minerals in shales and dolocretes.

Sample number	Phyllosilicates	Quartz	Calcite	Dolomite	Feldspar	Hematite	Gypsum	Rutile	Barite
<i>Shales</i>									
NT2	67	26	–	5	–	1	–	–	–
NT1	77	10	–	11	1	1	–	–	–
NP13	48	30	–	21	1	–	–	–	–
NP12	49	38	–	11	2	–	–	–	–
NP11	70	23	–	4	1	2	–	–	–
NP10	69	28	–	–	2	1	–	–	–
NP9	54	35	–	7	2	1	–	–	–
NP8	79	19	–	–	–	2	–	–	–
NP7	66	31	–	–	1	2	–	–	–
NP6	75	23	–	–	–	2	–	–	–
NP5	68	32	–	–	–	–	–	–	–
NP4	76	23	–	–	–	1	–	–	–
NP3	55	45	–	–	–	–	–	–	–
NP2	26	74	–	–	–	–	–	–	–
NP1	86	14	–	–	–	–	–	tr	–
ET7	80	5	14	–	1	–	–	–	–
ET6	86	7	–	6	–	1	–	–	–
ET5	79	9	8	3	–	1	–	–	–
ET4	71	9	–	12	1	1	6	–	–
ET3	79	7	–	10	–	–	4	–	–
ET2	81	9	9	–	–	1	–	–	–
ET1	79	8	13	–	–	–	–	–	–
GPP5	67	20	12	–	–	1	–	–	–
GPP4	57	33	8	–	1	1	–	–	–
GPP3	58	26	14	–	1	1	–	–	–
GPP2	84	11	2	3	–	1	–	–	–
GPP1	78	16	3	1	1	1	–	–	–
<i>Dolocretes</i>									
NTc6	16	5	–	79	–	–	–	–	–
NTc5	38	9	1	51	–	1	–	–	–
NTc4	10	24	2	64	–	–	–	–	–
NTc3	43	19	–	37	–	1	–	–	–
NTc2	32	22	6	38	1	1	–	–	–
NTc1	49	23	6	20	1	1	–	–	–
NPc8	28	10	–	62	–	–	–	–	–
NPc7	29	15	1	55	–	–	–	tr	–
NPc6	19	5	–	75	–	–	–	–	–
NPc5	31	10	2	56	–	1	–	–	–
NPc4	15	24	60	–	–	1	–	–	–
NPc3	13	7	–	80	–	–	–	–	tr
NPc2	36	14	–	49	–	1	–	–	–
NPc1	25	4	2	69	–	–	–	–	–

– is for “not detected”; tr = trace.

2.1. Permian–Triassic succession of northwestern Sardinia

The most complete Permian–Triassic succession in Sardinia is exposed at Nurra, in the northwestern sector of the island (Fig. 1). This succession is represented by at least three different continental sequences (Cassinis et al., 2003) that were deposited in a basin bounded to the north by a N130°-trending growth fault (Buzzi et al., 2008). The basin is hosted in upper greenschist metamorphic rocks that over a few kilometres pass into middle- and high-grade metamorphic rocks.

Several authors have studied the upper Palaeozoic–lower Mesozoic continental succession of Nurra from stratigraphic, sedimentological, and palaeontological points of view (Fontana et al., 2001; Cassinis et al., 2003; Ronchi et al., 2011). According to the latest work, the succession of the Nurra basin consists of three depositional cycles. The first cycle is represented by typical grey “Autunian” sediments (Ronchi et al., 2008) of the Punta Lu Caparoni Formation that overlie a thin basal conglomerate and that are overlain by black shales, sandstones, and cherty layers. Discontinuous ignimbrite dated at 291 Ma (Buzzi et al., 2008) occurs at the top. The second cycle is assigned to the lower Permian and represents the best-preserved portion of the whole Nurra succession. It is divided, from bottom to top, into the Cuile Pedru Siligu, Porto Ferro, and Cala del Vino formations, each of which is bounded by a noticeable regional unconformity. Overall,

these formations indicate a braided depositional environment evolving into a meandering system. Conglomerates and coarse sandstones with subordinate siltstones and shales are the main lithofacies, forming a general fining-upward succession. Within the upper part of the sequence, pelitic layers with mud cracks show typical pedogenic features highlighted by the presence of dolocretes and calcretes, bioturbation traces, and rhizolites. A regional-scale unconformity, resulting from a widespread late Permian–Early Triassic depositional hiatus, separates the second and third cycles. The third cycle starts with a 6 m thick, matrix-supported conglomerate (Conglomerato del Porticciolo Formation), which consists of decimetre scale, rounded and broken-rounded quartz clasts including wind-worn grains (Cassinis et al., 2003). Upwards, the sequence continues with the Cala Viola Formation, assigned to the lower Anisian (Pittau, 2002; Bourquin et al., 2007). This formation marks a clear change in facies: the cut-and-fill sedimentary structures typical of the Cala del Vino Formation are lacking, and the sedimentary structures are instead represented by medium-scale trough cross-bedding. However, lamination, climbing ripples (Ronchi et al., 2008), palaeosols, centimetre-sized caliche nodules, and dolocrete are all common. The latter constitute, as reworked intraclasts, the main component of decimetre-scale strata lying above palaeosols.

Among the aforementioned sediments, only siltstones and shales, and carbonate concretions (mainly dolocretes and calcretes) were

Table 2
Chemical composition of dolocretes.

Elements	NTc6	NTc5	NTc4	NTc3	NTc2	NTc1	NPc8	NPc7	NPc6	NPc5	NPc4	NPc3	NPc2	NPc1	Min.	Max.	Mean	σ
<i>wt.%</i>																		
SiO ₂	20.52	28.8	38.64	44.58	48.66	48.34	27.5	29.99	15.81	26.74	27.43	13.52	33.62	23.09	13.52	48.66	30.4	10.8
Al ₂ O ₃	4.59	6.92	2.64	9.2	8.38	9.53	6.15	7.53	3.25	7.85	6.25	3.04	9.06	6.08	2.64	9.53	6.6	2.3
Fe ₂ O ₃ (T)	1.96	2.63	1.18	2.43	2.51	2.85	4.74	3.03	1.82	6.10	2.06	1.89	5.29	6.77	1.18	6.77	3.2	1.7
MnO	0.31	0.20	0.20	0.13	0.11	0.09	0.73	0.51	0.88	0.70	0.01	1.12	0.50	0.50	0.01	1.12	0.4	0.3
MgO	14.63	11.56	11.3	8.35	6.32	4.65	10.3	11.11	15.23	9.98	1.04	14.76	9.08	10.93	1.04	15.23	9.4	4.4
CaO	20.92	17.73	17.86	12.3	12.14	12.3	18.14	16.87	23.28	17.37	32.94	24.7	14.48	18.67	12.14	32.94	19.3	6.1
Na ₂ O	0.12	0.16	0.07	0.23	0.54	0.42	0.09	0.24	0.08	0.10	0.17	0.10	0.13	0.55	0.07	0.55	0.2	0.2
K ₂ O	1.41	2.00	0.68	2.31	2.28	2.62	1.94	2.37	1.01	2.39	1.53	0.87	3.22	1.80	0.68	3.22	1.8	0.7
TiO ₂	0.25	0.38	0.16	0.51	0.49	0.56	0.27	0.34	0.19	0.34	0.30	0.17	0.43	0.18	0.16	0.56	0.3	0.1
P ₂ O ₅	0.07	0.07	0.04	0.04	0.07	0.06	0.02	0.03	0.04	0.03	0.1	0.005	0.02	0.06	0.01	0.10	0.0	0.0
LOI	33.59	27.79	27.17	20.87	19.32	17.92	28.55	27.58	36.85	27.79	27.82	36.79	23.65	31.28	17.92	36.85	27.6	5.6
Total	98.38	98.22	99.94	100.9	100.8	99.34	98.44	99.6	98.45	99.39	99.64	96.97	99.49	99.91	96.97	100.9	99.3	1.0
Mg/Ca	0.59	0.55	0.53	0.57	0.44	0.32	0.48	0.56	0.55	0.49	0.03	0.50	0.53	0.49	0.03	0.59	0.47	0.15
Calcif. Ind.	9.7	5.3	13.9	2.8	2.8	2.3	5.8	4.7	14.9	4.4	7.2	16.4	3.3	6.1	2.3	16.4	7.1	4.8
Hydr. Ind.	10.2	5.8	14.3	3.2	3.3	2.8	6.4	5.2	15.4	4.9	7.7	16.9	3.9	6.7	2.8	16.9	7.6	4.7
Salin. Ind.	0.08	0.07	0.09	0.09	0.21	0.14	0.04	0.09	0.07	0.04	0.10	0.10	0.04	0.27	0.04	0.27	0.10	0.07
<i>ppm</i>																		
Cr	10	20	10	30	30	30	20	30	40	30	20	10	20	10	10	40	22.0	9.4
V	35	44	23	47	54	57	32	72	41	54	45	25	53	65	23	72	46.1	13.8
Sc	5	7	3	8	8	8	7	22	21	9	6	16	25	32	3	32	12.4	8.6
Co	14	15	13	9	7	7	11	15	10	12	0.5	8	16	14	0.5	16	10.8	4.1
Ni	12	16	11	10	11	13	15	28	10	19	10	7	14	20	7	28	14.3	5.3
Zn	12	12	6	11	12	14	24	21	19	30	11	33	18	20	6	78	21.4	17.3
Cu	4	4	7	3	3	4	5	12	5	7	3	4	17	6	3	28	7.5	6.8
Cs	5.6	7	1.9	7.4	8.6	10.6	10.9	14.6	5.2	18.1	13.3	5.2	6.8	15	1.9	30	10.7	6.9
Ba	693	153	503	180	242	241	264	2994	293	233	1703	12040	400	2443	153	12040	1575.0	3028.5
Rb	48	68	23	80	82	98	70	85	37	97	61	36	64	76	23	98	65.7	22.2
Sr	123	134	59	90	138	154	62	132	62	89	244	141	43	83	43	244	115.2	53.3
Pb	2.5	8	2.5	2.5	2.5	7	2.5	2.5	2.5	2.5	2.5	2.5	11	2.5	2.5	24	5.2	5.8
Y	23	33	24	33	27	29	37	57	91	42	19	62	72	40	19	91	42.7	20.4
Th	5.7	8.4	4.7	12	11.7	13.8	10.8	11.1	21.8	10.6	6.3	3.3	15.8	6	3.3	21.8	10.1	4.8
U	1.8	2	1.1	3	2.4	2.8	1.5	1.7	2.4	1.4	2.4	0.8	2.7	0.8	0.8	3	1.9	0.7
Zr	82	153	77	234	245	265	134	102	69	109	96	49	118	38	38	265	123.8	71.0
Hf	2.1	3.9	2	5.9	5.9	6.9	3.5	2.7	2	2.8	2.5	1.4	3.2	1.1	1.1	6.9	3.2	1.7
Nb	5	8	3	11	10	12	6	7	4	7	6	4	10	4	3	12	6.9	2.8
La	23.7	34.3	17.9	35.0	31.6	37.1	31.7	20.8	16.5	37.2	16.8	20.1	23.2	24.4	16.5	53.7	28.3	10.2
Ce	43.9	51.0	25.4	65.8	63.6	74.9	52.6	42.2	40.1	60.4	34.0	37.5	56.3	50.3	25.4	74.9	51.3	14.4
Pr	5.5	8.0	4.7	8.4	7.2	8.5	8.0	6.0	5.7	9.0	3.8	5.1	7.8	6.1	3.79	11.3	7.0	2.0
Nd	19.5	29.0	17.1	29.6	25.9	30.2	31.1	23.5	24.4	33.6	13.5	20.7	33.3	23.9	13.5	42.1	26.5	7.3
Sm	4.2	6.3	3.7	6.3	5.2	6.0	7.2	7.1	8.8	8.0	2.8	6.1	10.3	6.8	2.8	10.3	6.6	2.1
Eu	0.8	1.3	0.8	1.3	0.9	1.1	1.6	2.0	3.3	1.7	0.5	2.0	2.9	1.9	0.49	3.29	1.6	0.8
Gd	4.0	6.1	3.6	5.7	4.4	5.3	7.6	9.4	13.0	7.7	2.8	8.2	12.7	8.8	2.8	13	7.3	3.1
Tb	0.7	1.1	0.7	1.1	0.8	0.9	1.3	2.0	3.0	1.2	0.5	1.7	2.6	1.5	0.5	3	1.4	0.7
Dy	4.1	6.2	4.1	6.5	4.8	5.6	6.8	11.7	19.0	7.3	3.2	10.7	15.4	8.8	3.2	19	8.3	4.4
Ho	0.8	1.2	0.8	1.3	0.9	1.1	1.3	2.2	3.7	1.4	0.7	2.1	3.0	1.5	0.7	3.7	1.6	0.9
Er	2.3	3.4	2.5	3.6	2.7	3.3	3.5	5.8	9.8	3.8	1.8	6.2	8.1	4.0	1.8	9.8	4.4	2.2
Tm	0.4	0.5	0.4	0.6	0.4	0.5	0.5	0.8	1.4	0.5	0.3	0.9	1.2	0.6	0.28	1.41	0.6	0.3
Yb	2.4	3.6	2.4	3.7	2.9	3.4	3.3	5.3	8.6	3.4	1.8	5.5	7.4	3.8	1.8	8.6	4.2	1.9
Lu	0.4	0.6	0.4	0.6	0.5	0.6	0.5	0.8	1.3	0.5	0.3	0.8	1.1	0.6	0.28	1.25	0.6	0.3
ΣREE	151.9	157.1	152.6	169.4	178.5	175.8	112.6	84.5	139.6	158.5	82.7	127.6	185.3	143.0	82.7	226.6	149.7	37.8
Ce/Ce*	0.96	0.76	0.70	0.88	0.96	0.75	0.88	0.64	0.88	0.97	0.97	0.85	0.98	0.95	0.64	0.98	0.9	0.1
Eu/Eu*	0.59	0.66	0.62	0.64	0.59	0.65	0.63	0.64	0.76	0.94	0.53	0.84	0.78	0.74	0.47	0.94	0.7	0.1
(La/Yb) _N	7.36	6.49	6.44	6.39	7.37	7.39	6.67	5.04	2.65	1.30	6.31	2.47	2.12	4.34	1.30	7.39	5.3	2.1

Calcif. Ind. = calcification index: (CaO + MgO)/Al₂O₃; Hydr. Ind. = hydrolysis index: (CaO + MgO + K₂O + Na₂O)/Al₂O₃; Salin. Ind. = salinisation index: Na₂O/K₂O. Min., Max., Mean, and σ refer to the minimum, maximum, mean, and standard deviation values, respectively.

regarded as suitable subjects for the purposes of this research. They were sampled for mineralogical and geochemical analyses.

2.2. Permian and Triassic successions of southern Sardinia

Continental sediments of Triassic age, comparable with those of Nurra (Pecorini, 1974), occur in the central and southeastern areas of Sardinia, namely Escalaplano and Guardia Pisano (Fig. 1). The Escalaplano Formation represents the base of the Triassic sedimentary cycle of southeastern Sardinia, which is developed from the upper Anisic to lower Ladinian (Costamagna et al., 2000). This formation is divided into four lithofacies that define a fining-upward trend. Upwards through the sequence, coarse sediments of an alluvial fan system show a transition to a 20 m thick alternation of thin plane-parallel clayey, silty and marly layers. Gypsum deposits, indicating an alluvial plain depositional environment where ephemeral lakes and/or weakly evaporite lagoons formed, mark the top of the sequence.

The final group of clastic deposits considered in this paper belongs to the Guardia Pisano Basin, which is located in the external zone of the chain (close to the foreland), likely bounded by a collisional backthrust (Funedda, 2009) that acts as low-angle normal fault. These lower–middle Permian deposits are composed of sediments similar to the Permian and Triassic red beds of the Nurra and Escalaplano basins. Detailed stratigraphic descriptions and facies analysis of the Guardia Pisano succession were made by Barca and Costamagna (2006) and Ronchi et al. (2008), who subdivided the succession into three and four lithostratigraphic units, respectively, describing a discontinuous volcano-sedimentary succession interrupted by high stratigraphic gaps. The succession comprises conglomerate and micro-conglomerate layers or lenses within thick sandstones and siltstone red beds. The sampled shales and siltstones characterise the lithofacies D, sensu Ronchi et al. (2008), which is composed of grey to red sandstones and shales typical of a floodplain depositional system.

3. Sampling and methods

Fortyone samples were collected from the bottom to the top of the sequences described above (Fig. 2). As shown in Fig. 2, most of the samples were taken from the Nurra succession due to its widespread exposure. Twenty-seven samples were shales and sandstones. Of these, 15 were collected from the Permian–Triassic Nurra succession (NT and NP samples), seven were from the Triassic Escalaplano succession (ET), and five from the Permian Guardia Pisano sediments (GPP). Fourteen samples were carbonate concretions developed within shales of the Nurra succession (NTc and NPc based on their Triassic or Permian age) and locally associated with palaeosol horizons (dolocretes or calcretes).

All samples were first dried and then milled in a planetary mill (Retsch) equipped with two agate jars and agate milling balls to obtain a very fine powder suitable for the chemical and mineralogical analyses. Whole-rock mineralogy was determined by X-ray powder diffraction (XRPD) using a Siemens D5000 powder diffractometer (Cu-K α radiation, 40 kV, 30 mA, step size 0.02° (2 θ)). Quantitative mineralogical analysis was performed on random powders by measuring peak areas using DIFFRAC^{plus} EVA software (Bruker AXS). The strongest reflection of each mineral was considered, except for quartz for which the line at 4.26 Å was used instead of the peak at 3.34 Å to avoid superimposition with the 10-Å mineral peak. Following Laviano (1987) and Cavalcante et al. (2007), the amount of phyllosilicates (clay minerals and muscovite) was estimated by measuring the 4.5 Å peak area. Elemental analyses for major, trace, and rare earth element concentrations were obtained by inductively coupled plasma–mass spectrometry (ICP-MS) and instrumental neutron activation analysis (INAA) at Activation Laboratories (Ancaster, Canada). Analytical uncertainties were less than $\pm 5\%$, except for those elements occurring at a concentration of 10 ppm or lower, for which the uncertainties were

$\pm 5\%$ –10%. Total loss on ignition (LOI) was gravimetrically estimated after overnight heating at 950 °C. W-2a, DNC-1, BIR-1a, LKSD-3, WMG-1, NCS DC700009 (GBW 07241), NCS DC70014, NCS DC86312, OREAS 100a, OREAS 101a, CTC-AC-1, TDB-1, GXR-2, and JR-1 are the standard reference materials that were used for the instrumental calibration and direct rock comparison.

The texture, mineralogy, and microchemistry of polished sections of representative samples were analyzed using an EVO LS10 Zeiss LaB₆ environmental scanning electron microscope (ESEM) equipped with an energy dispersion spectrometer (EDS). Before applying palaeoweathering proxies to the analyzed red beds, the CaO fraction related to carbonate phases (calcite and dolomite detected and quantified by XRD analysis) was extracted from the measured CaO percentage of all samples.

4. Results

The mineralogical and chemical data of the analyzed sediments are presented in Tables 1–3 respectively. These data refer to the siltstones and shales of the three studied successions and to the dolocrete and carbonate concretions of Nurra. The data have been arranged according to the stratigraphic positions of samples, from the top to the bottom of the successions.

4.1. Whole-rock mineralogy

4.1.1. Carbonate concretions

The carbonate concretions sampled from the Triassic and Permian Nurra shales show a mineralogical association dominated by carbonates (calcite and dolomite) and silicate minerals (clay minerals and quartz). Very high contents of dolomite and minor calcite were detected in all samples. Dolomite makes up 20%–79% of the Triassic samples and 49%–75% of the Permian samples. Calcite is found chiefly in microscopic veins cross-cutting both dolomite and Fe oxides, making up 1%–6% and 1%–2% of the rock mass, respectively, in Triassic and Permian concretions, except for the sample NPc4 in which the calcite content is 60%. In most of the concretions, scarce amounts of Fe oxide (hematite, 1%) are also found. Very low percentages of feldspar (1%) are observed in two Triassic concretions (NTc2 and NTc1). Barite content is below 1% and locally is concentrated in centimetre-scale crystals and rosettes. Traces of rutile are also found in the samples NPc3 and NPc7. ESEM-EDS analyses of the Triassic samples show dolomite concretions rimmed by radial intergrowths of dolomite and mostly dissolved, ghost-mineral phases (most likely chlorides) rich in Cl, Mg, and Ca. Because of their very similar compositions and to simplify discussion, the carbonate concretions of the Nurra succession are herein regarded as dolocretes.

4.1.2. Siliciclastic sediments

The Permian and Triassic siltstones and shales of the sedimentary basins of northwestern and southern Sardinia are characterised by similar mineralogical compositions. The Triassic sediments of the Nurra succession are composed of phyllosilicates (such as illite and muscovite) and quartz as the main mineral phases (Table 1). Dolomite is the sole carbonate phase in these samples. Feldspars (mainly plagioclase and K-feldspar) and hematite occur as accessory minerals.

The Triassic shales of the Escalaplano Basin, as well as those of Nurra, are composed mainly of phyllosilicates (mostly illite and muscovite) predominant over quartz, calcite, and/or dolomite, and hematite and minor amounts of feldspars. Phyllosilicates are the main minerals in the shales (71%–86%). Quartz (ranging from 5% to 9%), calcite (ranging from 8% to 14%), and dolomite (3% and 12%) are the most abundant phases among the non-phyllosilicate minerals. Hematite and feldspars are scarce and their concentrations do not exceed 1%. Two samples contain gypsum (ET4 = 7% and ET3 = 5%).

The Permian siliciclastic sediments of the Nurra succession show a mineralogical composition including only phyllosilicates (26% to 86%)

Table 3
Chemical composition of shales.

Elements	Nurra Basin samples															Min.	Max.	Mean	σ
	NT2	NT1	NP13	NP12	NP11	NP10	NP9	NP8	NP7	NP6	NP5	NP4	NP3	NP2	NP1				
wt.%																			
SiO ₂	68.45	53.97	57.76	64.61	60.92	57.76	64.61	60.78	60.26	60.92	82.08	75.30	84.85	88.12	64.41	53.97	88.12	67.0	10.6
Al ₂ O ₃	11.94	15.69	9.79	12.46	16.49	9.79	12.46	19.02	18.34	16.49	11.21	14.21	8.98	6.26	22.06	6.26	22.06	13.7	4.3
Fe ₂ O ₃ (T)	3.75	5.89	2.55	2.67	6.35	2.55	2.67	7.38	7.12	6.35	0.53	1.55	0.52	1.92	0.56	0.52	7.38	3.5	2.5
MnO	0.05	0.07	0.24	0.11	0.06	0.24	0.11	0.03	0.03	0.06	0.01	0.02	0.01	0.05	0.11	0.01	0.24	0.1	0.1
MgO	1.91	3.21	4.71	2.41	1.81	4.71	2.41	1.29	1.24	1.81	0.34	0.44	0.29	0.17	0.30	0.17	4.71	1.8	1.5
CaO	1.94	3.44	7.76	3.65	1.30	7.76	3.65	0.38	0.39	1.30	0.29	0.50	0.19	0.07	0.31	0.07	7.76	2.2	2.6
Na ₂ O	0.25	0.24	0.13	0.16	0.18	0.13	0.16	0.21	0.51	0.18	0.10	0.10	0.11	0.10	0.18	0.10	0.51	0.2	0.1
K ₂ O	3.61	4.99	2.78	3.63	5.10	2.78	3.63	5.29	4.92	5.10	2.76	3.47	2.41	1.33	2.66	1.33	5.29	3.6	1.2
TiO ₂	0.75	0.78	0.44	0.61	0.79	0.44	0.61	0.77	0.79	0.79	0.44	0.56	0.34	0.20	1.06	0.20	1.06	0.6	0.2
P ₂ O ₅	0.07	0.14	0.04	0.06	0.08	0.04	0.06	0.13	0.07	0.08	0.22	0.42	0.14	0.04	0.25	0.04	0.42	0.1	0.1
LOI	6.49	9.75	14.41	8.70	6.60	14.41	8.70	5.63	5.84	6.60	2.74	3.61	2.35	2.18	6.87	2.18	14.41	7.0	3.8
Total	99.18	98.17	100.60	99.08	99.68	100.60	99.08	100.90	99.51	99.68	100.70	100.20	100.20	100.40	98.78	98.17	100.90	99.8	0.8
ClA	65	65	60	66	66	72	68	67	68	70	70	69	68	73	82	60	82	68.6	4.9
ClW	93	96	82	95	97	98	96	94	96	98	96	95	96	96	97	82	98	94.9	3.8
ICV	1.1	1.2	1.1	0.9	1.2	0.9	1.0	1.1	1.1	1.0	0.6	0.7	0.6	0.9	0.3	0.3	1.2	0.9	0.3
ppm																			
Cr	40	60	20	40	60	60	50	70	70	60	60	70	40	20	140	20	140	57.3	28.1
V	62	86	51	66	104	86	70	109	105	90	70	95	57	50	84	50	109	79.0	19.7
Sc	11	14	12	9	13	12	11	16	16	13	7	12	7	5	7	5	16	11.0	3.4
Co	5	9	16	11	8	7	11	9	12	8	6	24	3	3	8	3	24	9.3	5.3
Ni	21	27	24	24	33	21	24	39	36	32	17	52	13	13	39	13	52	27.7	10.8
Zn	21	27	23	24	41	35	34	70	80	65	27	27	16	7	9	7	80	33.7	21.8
Cu	7	5	10	12	13	19	19	15	12	13	32	53	16	6	22	5	53	16.9	12.1
Cs	12.0	21.5	10.5	18.1	34.3	26.5	20.2	59.0	59.7	50.0	14.0	14.4	11.3	6.6	10.7	6.6	59.7	24.6	17.9
Ba	234	371	3437	3574	1345	365	554	424	399	398	253	265	215	159	214	159	3574	813.8	1128.9
Rb	122	181	82	123	195	170	142	250	229	218	121	145	95	56	98	56	250	148.5	57.2
Sr	138	166	101	124	145	59	76	146	121	113	75	119	56	54	87	54	166	105.3	36.0
Pb	8	7	2.5	2.5	16	13	10	25	24	17	66	97	27	2.5	6	2.5	97	21.6	26.3
Y	33	30	29	30	31	27	28	34	30	29	21	35	15	11	41	11	41	28.3	7.6
Th	17.6	16.7	10.9	15.8	15.4	18.9	14.6	18.5	16.5	17.6	10.5	13.4	7.8	4.7	18.6	4.7	18.9	14.5	4.3
U	5.1	4.1	3.5	4.3	4	5.2	4.1	3.2	3.1	3.2	2.6	2.9	1.8	3.3	3.9	1.8	5.2	3.6	0.9
Zr	404	241	183	305	217	349	263	155	175	211	109	137	77	51	224	51	404	206.7	97.6
Hf	9.8	6.3	4.4	7.4	5.4	8.6	6.8	4.2	4.5	5.7	2.5	3.4	1.8	1.1	5.9	1.1	9.8	5.2	2.4
Nb	15	17	8	11	17	15	11	19	18	17	8	10	5	3	16	3	19	12.7	5.0
Zr/Sc	36.7	17.2	15.3	33.9	16.7	29.1	23.9	16.2	9.7	10.9	15.6	11.4	11.0	10.2	32.0	9.7	36.7	19.3	9.3
Th/Sc	1.6	1.2	0.9	1.8	1.2	1.6	1.3	1.4	1.2	1.0	1.5	1.1	1.1	0.9	2.7	0.91	2.66	1.4	0.4
V/Cr	1.6	1.4	2.6	1.7	1.7	1.4	1.4	1.5	1.6	1.5	1.2	1.4	1.4	2.5	0.6	0.60	2.55	1.6	0.5
La	48.8	48.7	23.1	43.4	44.3	45.5	41.4	48.3	40.8	43.6	26.4	49.4	18.4	24.2	41.3	18.4	49.4	39.2	10.6
Ce	95.8	87.8	46.1	89.1	89.6	89.7	82.0	98.7	81.8	85.5	50.6	102.0	36.3	42.9	80.6	36.3	102.0	77.2	21.8
Pr	11.0	10.2	5.4	9.9	9.8	9.9	9.4	11.0	8.9	9.3	5.9	12.0	4.1	4.7	9.5	4.1	12.0	8.7	2.5
Nd	38.4	34.8	19.9	34.6	34.4	33.6	32.7	37.8	30.1	32.3	21.3	44.8	14.8	17.6	35.7	14.8	44.8	30.9	8.6
Sm	7.3	6.9	4.9	6.8	6.6	6.4	6.6	7.8	5.8	6.1	4.3	9.8	3.3	3.1	7.4	3.1	9.8	6.2	1.7
Eu	1.2	1.3	1.0	1.1	1.2	0.9	1.1	1.5	1.1	1.1	1.0	2.2	0.7	0.7	1.6	0.7	2.2	1.2	0.4
Gd	5.9	5.9	5.2	6.2	5.5	4.8	5.4	6.1	4.7	4.6	4.3	9.8	3.1	2.5	7.7	2.5	9.8	5.4	1.7
Tb	1.1	1.1	1.0	1.0	0.9	0.9	0.9	1.1	0.9	0.8	0.8	1.6	0.5	0.4	1.3	0.4	1.6	1.0	0.3
Dy	6.0	6.2	5.9	6.0	5.5	5.3	5.6	6.2	5.6	5.2	4.1	8.2	3.0	2.0	7.7	2.0	8.2	5.5	1.6
Ho	1.2	1.2	1.1	1.2	1.1	1.1	1.1	1.3	1.1	1.1	0.8	1.4	0.6	0.4	1.5	0.4	1.5	1.1	0.3
Er	3.6	3.4	2.9	3.4	3.2	3.2	3.2	3.7	3.2	3.3	2.2	3.6	1.6	1.3	4.2	1.3	4.2	3.1	0.8
Tm	0.55	0.56	0.45	0.51	0.5	0.51	0.5	0.55	0.5	0.5	0.32	0.49	0.24	0.19	0.61	0.2	0.6	0.5	0.1
Yb	3.7	3.5	3	3.3	3.4	3.5	3.3	3.6	3.3	3.4	2.1	2.9	1.6	1.3	3.9	1.3	3.9	3.1	0.8
Lu	0.6	0.6	0.5	0.6	0.5	0.6	0.5	0.6	0.5	0.6	0.3	0.4	0.3	0.2	0.6	0.2	0.6	0.5	0.1
ΣREE	225.1	212.1	120.4	207.0	206.5	205.9	193.7	228.2	188.2	197.3	124.4	248.6	88.5	101.5	203.7	88.5	248.6	183.4	49.5
Ce/Ce*	0.94	0.89	0.94	0.98	0.98	0.96	0.95	0.97	0.97	0.96	0.92	0.96	0.95	0.89	0.93	0.89	0.98	0.9	0.0

	0.54	0.63	0.58	0.49	0.58	0.52	0.54	0.66	0.62	0.62	0.68	0.68	0.68	0.72	0.66	0.49	0.72	0.6	0.1	
(La/Yb) _N	8.91	9.40	5.20	8.89	8.80	8.78	8.48	9.07	8.35	8.67	8.50	11.51	7.77	12.58	7.16	5.20	12.58	8.8	1.7	
(Gd/Yb) _N	1.3	1.4	1.4	1.5	1.3	1.1	1.3	1.1	1.4	1.2	1.7	2.7	1.6	1.6	1.6	1.1	2.7	1.5	0.4	
Elements	Escalaplano Basin samples											Guardia Pisano Basin samples								
	ET7	ET6	ET5	ET4	ET3	ET2	ET1	Min.	Max.	Mean	σ	GPP5	GPP4	GPP3	GPP2	GPP1	Min.	Max.	Mean	σ
wt.%																				
SiO ₂	48.22	47.63	48.73	46.16	51.05	49.66	49.09	46.16	51.05	48.6	1.5	60.35	63.37	62.87	55.55	60.90	55.55	63.37	60.6	3.1
Al ₂ O ₃	12.06	18.11	13.96	15.23	15.81	18.19	17.69	12.06	18.19	15.9	2.3	12.35	11.78	9.10	17.34	17.78	9.10	17.78	13.7	3.8
Fe ₂ O ₃ (T)	2.26	7.80	8.64	9.30	5.38	5.85	5.87	2.26	9.30	6.4	2.4	5.15	5.25	4.10	5.39	4.93	4.10	5.39	5.0	0.5
MnO	0.02	0.08	0.06	0.07	0.05	0.06	0.10	0.02	0.10	0.1	0.0	0.07	0.07	0.15	0.05	0.03	0.03	0.15	0.1	0.0
MgO	5.55	6.21	4.35	5.46	5.71	3.49	3.43	3.43	6.21	4.9	1.1	0.84	0.80	0.61	2.69	1.35	0.61	2.69	1.3	0.8
CaO	8.33	1.88	5.50	3.90	3.05	5.38	7.30	1.88	8.33	5.0	2.3	7.62	6.50	9.36	4.00	3.02	3.02	9.36	6.1	2.6
Na ₂ O	0.13	0.23	0.23	0.21	0.25	0.14	0.24	0.13	0.25	0.2	0.0	0.35	0.21	0.22	0.27	0.21	0.21	0.35	0.3	0.1
K ₂ O	6.97	5.43	4.27	4.77	4.97	4.44	4.20	4.20	6.97	5.0	1.0	2.44	2.33	1.75	3.51	2.94	1.75	3.51	2.6	0.7
TiO ₂	0.20	0.72	0.63	0.66	0.70	0.53	0.55	0.20	0.72	0.6	0.2	0.63	0.63	0.49	0.62	0.61	0.49	0.63	0.6	0.1
P ₂ O ₅	0.05	0.21	0.17	0.20	0.20	0.29	0.24	0.05	0.29	0.2	0.1	0.11	0.12	0.10	0.20	0.13	0.10	0.20	0.1	0.0
LOI	15.61	12.42	11.92	12.44	11.61	10.66	11.38	10.66	15.61	12.3	1.6	10.77	9.17	11.17	11.19	8.93	8.93	11.19	10.2	1.1
Total	99.40	100.70	98.45	98.40	98.79	98.72	100.10	98.40	100.70	99.2	0.9	100.70	100.20	99.93	100.80	100.80	99.93	100.80	100.5	0.4
ClA	51	67	66	65	66	71	72	51	72	65.3	6.9	69	65	64	66	74	64	74	67.5	3.8
ClW	94	98	97	96	97	97	98	94	98	96.5	1.5	87	81	80	84	91	80	91	84.5	4.6
ICV	1.8	1.4	1.7	1.6	1.3	1.1	1.1	1.1	1.8	1.4	0.3	1.2	1.3	1.3	1.1	0.8	0.8	1.3	1.1	0.2
ppm																				
Cr	10	80	70	70	70	70	80	10	80	64.3	24.4	50	40	40	50	50	40	50	46.0	5.5
V	31	132	117	129	125	152	121	31	152	115.3	38.8	98	85	66	98	90	66	98	87.4	13.2
Sc	12	16	13	14	15	18	17	12	18	15.0	2.2	11	11	9	14	12	9	14	11.4	1.8
Co	2	19	16	15	22	14	15	2	22	14.7	6.3	8	8	7	15	9	7	15	9.4	3.2
Ni	6	48	37	38	45	32	37	6	48	34.7	13.8	28	28	25	39	29	25	39	29.8	5.4
Zn	25	138	111	112	127	94	105	25	138	101.7	36.8	78	77	64	129	99	64	129	89.4	25.4
Cu	70	18	11	11	105	18	51	11	105	40.6	36.3	19	21	23	26	18	18	26	21.4	3.2
Cs	29.6	46.9	34.7	41.6	37.7	17.3	17.7	17	47	32.2	11.4	51.4	52.4	38.3	80.2	81.6	38	82	60.8	19.2
Ba	218	548	482	460	491	586	631	218	631	488.0	133.8	362	523	294	439	475	294	523	418.6	91.1
Rb	172	222	166	180	187	208	197	166	222	190.3	20.0	113	109	80	177	158	80	177	127.4	39.3
Sr	36	73	72	142	345	179	305	36	345	164.6	120.1	121	118	102	429	258	102	429	205.6	139.8
Pb	13	2.5	9	8	7	8	2.5	3	13	7.1	3.7	20	21	26	35	32	20	35	26.8	6.6
Y	10	23	21	21	22	19	20	10	23	19.4	4.4	25	24	25	32	32	24	32	27.6	4.0
Th	14.6	13.2	11.1	11.5	12.8	11.5	10.6	11	15	12.2	1.4	10.5	10.6	8.8	17.5	18.1	9	18	13.1	4.4
U	3.1	3	3.2	3.7	3.9	2.8	3	3	4	3.2	0.4	2.3	2.2	1.9	2.4	1.6	2	2	2.1	0.3
Zr	145	109	116	113	127	92	88	88	145	112.9	19.6	184	205	192	119	132	119	205	166.4	38.4
Hf	4.7	2.7	2.8	2.8	3.2	2.4	2.3	2	5	3.0	0.8	4.6	4.9	4.9	3.2	3.6	3	5	4.2	0.8
Nb	6	12	9	10	11	7	9	6	12	9.1	2.1	12	12	9	14	15	9	15	12.4	2.3
Zr/Sc	12.1	6.8	8.9	8.1	8.5	5.1	5.2	5.1	12.1	7.8	2.4	16.7	18.6	21.3	8.5	11.0	8.5	21.3	15.2	5.3
Th/Sc	1.2	0.8	0.9	0.8	0.9	0.6	0.6	0.6	1.2	0.8	0.2	1.0	1.0	1.0	1.3	1.5	1.0	1.5	1.1	0.2
V/Cr	3.1	1.7	1.7	1.8	1.8	2.2	1.5	1.5	3.1	2.0	0.5	2.0	2.1	1.7	2.0	1.8	1.7	2.1	1.9	0.2
La	14.3	35.1	33.7	34.9	35.2	27.9	24.9	14.3	35.2	29.4	7.8	31.8	31.2	27.7	32.2	34.9	27.7	34.9	31.6	2.6
Ce	31.7	72.2	67.8	69.6	71.1	55.3	49.4	31.7	72.2	59.6	15.1	63.4	62.1	57.7	74.0	74.4	57.7	74.4	66.3	7.5
Pr	3.3	8.0	7.4	7.5	8.2	6.3	5.6	3.3	8.2	6.6	1.7	7.2	6.9	6.5	8.7	8.1	6.5	8.7	7.5	0.9
Nd	11.6	30.5	27.7	28.4	30.3	25.1	21.9	11.6	30.5	25.1	6.7	25.6	24.5	23.8	32.4	29.4	23.8	32.4	27.1	3.6
Sm	2.2	6.2	5.3	5.6	5.9	5.2	4.6	2.2	6.2	5.0	1.3	5.3	4.9	5.1	7.4	6.0	4.9	7.4	5.7	1.0
Eu	0.3	1.2	1.0	1.2	1.1	1.0	0.9	0.3	1.2	1.0	0.3	1.0	0.9	1.0	1.2	0.9	0.9	1.2	1.0	0.1
Gd	1.7	4.8	4.4	4.5	4.7	4.3	4.1	1.7	4.8	4.1	1.1	4.6	4.3	4.8	6.6	5.3	4.3	6.6	5.1	0.9
Tb	0.3	0.8	0.7	0.7	0.8	0.7	0.7	0.3	0.8	0.7	0.2	0.8	0.8	0.9	1.2	1.0	0.8	1.2	0.9	0.2
Dy	2.0	4.2	3.9	4.0	4.5	3.8	3.9	2.0	4.5	3.8	0.8	4.9	4.6	4.8	6.6	5.8	4.6	6.6	5.3	0.8
Ho	0.4	0.8	0.8	0.8	0.9	0.8	0.8	0.4	0.9	0.8	0.2	1	0.9	0.9	1.2	1.2	0.9	1.2	1.0	0.2
Er	1.3	2.3	2.2	2.2	2.4	2.2	2.1	1.3	2.4	2.1	0.4	2.7	2.5	2.6	3.4	3.3	2.5	3.4	2.9	0.4
Tm	0.22	0.37	0.35	0.36	0.38	0.34	0.34	0.22	0.38	0.3	0.1	0.4	0.39	0.38	0.51	0.51	0.38	0.51	0.4	0.1
Yb	1.6	2.3	2.3	2.3	2.5	2.3	2.4	1.6	2.5	2.2	0.3	2.6	2.5	2.5	3.4	3.3	2.5	3.4	2.9	0.5

(continued on next page)

Table 3 (continued)

Elements	Escalaplano Basin samples											Guardia Pisano Basin samples								
	ET7	ET6	ET5	ET4	ET3	ET2	ET1	Min.	Max.	Mean	σ	GPP5	GPP4	GPP3	GPP2	GPP1	Min.	Max.	Mean	σ
Lu	0.3	0.4	0.4	0.4	0.4	0.4	0.4	0.3	0.4	0.4	0.0	0.4	0.4	0.4	0.5	0.5	0.4	0.5	0.5	0.1
Σ REE	71.1	169.2	157.9	162.4	168.3	135.6	121.9	71.1	169.2	140.9	35.5	151.7	147.0	139.1	179.3	174.7	139.1	179.3	158.4	17.7
Ce/Ce*	1.06	0.98	0.97	0.97	0.96	0.95	0.95	0.95	1.06	1.0	0.0	0.95	0.96	0.98	1.03	1.01	0.95	1.03	1.0	0.0
Eu/Eu*	0.49	0.69	0.65	0.70	0.64	0.61	0.63	0.49	0.70	0.6	0.1	0.62	0.61	0.64	0.54	0.51	0.51	0.64	0.6	0.1
(La/Yb) _N	6.04	10.31	9.90	10.25	9.51	8.20	7.01	6.04	10.31	8.7	1.7	8.26	8.43	7.49	6.40	7.15	6.40	8.43	7.5	0.8
(Gd/Yb) _N	0.9	1.7	1.6	1.6	1.5	1.5	1.4	0.9	1.7	1.4	0.3	1.4	1.4	1.6	1.6	1.3	1.3	1.6	1.5	0.1

Min., Max., Mean, and σ refer to the minimum, maximum, mean, and standard deviation values respectively.

and quartz (14% to 74%) as the main mineral phases. Dolomite is the sole carbonate in these sediments and is found in the samples from the top of the succession (from samples NP9 to NP13); it ranges from 4% to 11%, except for sample NP13, which contains 21% of dolomite. Feldspars are mainly present in the samples of the upper part of the Permian Nurra section with lower concentrations than those of carbonate (from 1% to 2%). Hematite also occurs in most of the samples through the whole succession (1%–2%).

The samples of Guardia Pisano succession have similar mineral assemblages to each other, composed by phyllosilicates and quartz as the main phases, and calcite and hematite as accessory phases. Few amounts of feldspars are observed in most samples (GPP4, GPP3, GPP1 = 1%), and few amounts of dolomite are detected in two samples (GPP2 = 3% and GPP1 = 1%).

4.2. Chemistry

4.2.1. Dolocretes

SiO₂, CaO, and MgO are the most abundant major elements in the dolocretes. The samples are characterised by Al₂O₃ contents ranging from 2.64 to 9.53 wt.% and Fe₂O₃ contents ranging from 1.18 to 6.77 wt.%. The average K₂O content is 1.8 wt.%. The concentrations of the remaining major elements (MnO, Na₂O, TiO₂, and P₂O₅) are consistently lower than 1 wt.%. The SiO₂–MgO–CaO ternary plot (Fig. 3) shows that these deposits, with the exception of sample NPc4, can be regarded as a mixture of dolomite and quartz, in agreement with the mineralogical data. The distribution of the Mg/Ca ratio through the Nurra succession (Fig. 4) indicates that this index is affected by minor changes, fluctuating between 0.44 and 0.59 with the exceptions of sample NPc4 (Mg/Ca = 0.03), which is devoid of dolomite, and sample NTc1 (Mg/Ca = 0.32), which has a low dolomite content.

Molecular weight ratios are also used to describe the features of carbonate palaeosols (Retallack, 1997, 2001). The ratio of alkaline earths to alumina [(CaO + MgO)/Al₂O₃], which functions as a calcification index, ranges from 3.3 to 16.4 in the Permian samples and from 2.3 to 13.9 in the Triassic samples (Fig. 5). The base/alumina ratio [(CaO + MgO + K₂O + Na₂O)/Al₂O₃] defines the former hydrolysis conditions of palaeosol formation and, due here to the very low contents of both K₂O and Na₂O, shares the same behaviour as the alkaline earths/alumina ratio, ranging from 3.9 to 16.9 for the Permian samples and from 2.8 to 14.3 for the Triassic samples (Fig. 5). Finally, the Na₂O/K₂O ratio, which is useful for defining the degree of soil salinisation, lies well below 1 for all the samples (Fig. 5).

The dolocretes are characterised by a wide compositional variability of the trace elements distribution and, as expected, are generally depleted with respect to the PAAS (Post-Archean Australian Shale; Taylor and McLennan, 1985) composition. Only Cs, Y, Sc, and Ba show a different behaviour in few samples. Due to the high contents of carbonate minerals, which have a dilution effect on most elements, the total amount of rare earth elements (REEs), which are hosted in the detrital component, is low, ranging from 82 to 186 ppm. Chondrite-normalised REE patterns are generally flat (Fig. 6) as the light REE/heavy REE (LREE/HREE) fractionation index lies well below 10 in most samples (see Table 2). The Triassic samples generally display larger negative Eu anomalies (Eu/Eu* = 0.59–0.64) than those of the Permian samples (Eu/Eu* = 0.53–0.94). Overall, the samples, despite their age, show slightly negative Ce anomalies that are more pronounced in some samples: NPc5, NPc8, NTc4, and NTc5.

4.2.2. Permian and Triassic siliciclastic sediments

Regarding the chemical composition of the studied shales, the wide range of CaO contents (0.10–9.36 wt.%) appears on first inspection to be a major feature. However, although most samples are enriched in CaO, the SiO₂–Al₂O₃–CaO ternary plot (Fig. 3) shows that the sediments fall close to the models of the upper continental crust composition, PAAS, and GLOSS (Global Subducting Sediment; Plank and Langmuir, 1998).

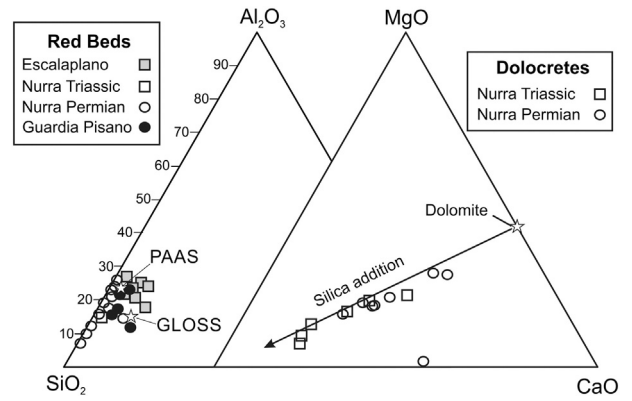


Fig. 3. SiO₂–MgO–CaO ternary plot for siliciclastic and carbonate samples. Diagrams suggest both an upper continental crust-type composition for red beds and a silica addition trend for dolocretes. PAAS, Post-Achaean Australian Shales; GLOSS, Global Subducting Sediment.

Their chemical properties are thus simply related to the relative proportions of SiO₂ and Al₂O₃, and most samples, especially those from the Nurra Basin, fall close to the SiO₂–Al₂O₃ join towards the silica apex.

To better examine the geochemical features of the studied samples, we calculated and interpreted the enrichment factors for major and trace elements (see Hassan et al., 1999 and references therein) relative to the PAAS (Table 4). The enrichment factor for a given element (e), hereafter called F_(e), is calculated as

$$F_{(e)} = (C_e \text{ sample} / C_{Al} \text{ sample}) / (C_e \text{ PAAS} / C_{Al} \text{ PAAS}),$$

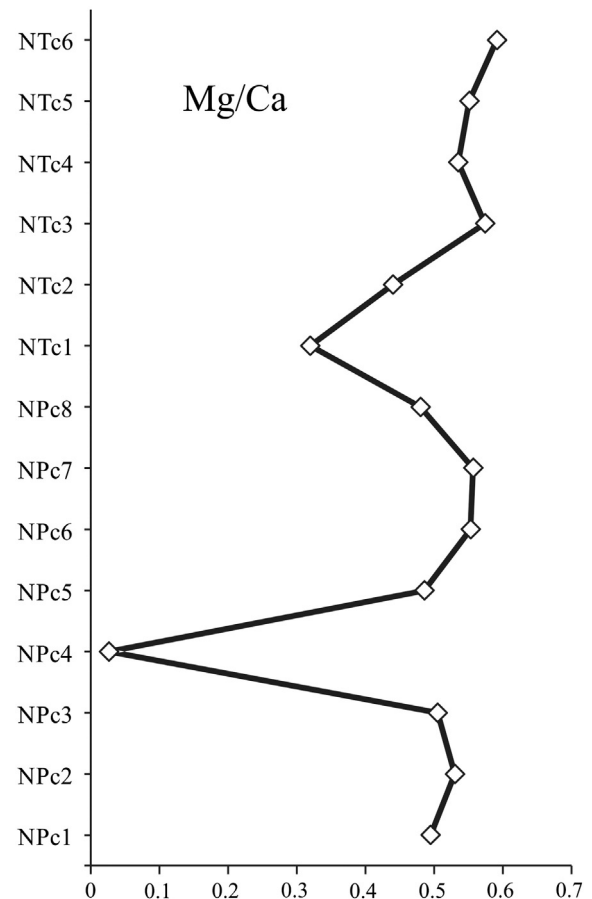


Fig. 4. Distribution of the Mg/Ca ratio through the Nurra succession. See text for further details.

where C_e is the concentration of the element and C_{Al} is the concentration of Al, used as a normalizing element. The elements considered in the analysis were grouped on the basis of their behaviour, and are discussed in turn below in relation to their stratigraphic variations.

SiO₂. The silica distribution is characterised by minor fluctuations, with F_{SiO_2} values that are generally close to 1. A notable exception is observed in the basal part of the Nurra succession, in the time interval ranging from NP2 to NP5, where F_{SiO_2} is well above 1; this is especially true for level NP2, where F_{SiO_2} measures 4.2.

CaO and MgO. The highest upper Permian samples associated with the Guardia Pisano Basin are characterised by high F_{CaO} values (up to about 15) and F_{MgO} values usually well below 1 (Fig. 7). CaO and MgO, both in the Nurra Basin samples (which are mostly Permian in age) and in the Triassic samples from the Escalaplano Basin, share the same stratigraphic distribution. In the upper Permian samples, both F_{CaO} and F_{MgO} are well below 1. In the lower Permian samples, there is an increase in both F_{CaO} and F_{MgO} that, in the uppermost Permian sample (NP13), show very high values of $F_{CaO} = 11.5$ and $F_{MgO} = 4.1$. In the Triassic samples, from both the Nurra Basin and the Escalaplano Basin, the CaO and MgO enrichment factors are always well above 1. As the correlations between CaO and SiO₂ ($r = -0.82$) and MgO and SiO₂ ($r = -0.90$) indicate that CaO and MgO are hosted predominantly in calcite and dolomite, which is in agreement with the mineralogical composition, the overall variability of F_{CaO} and F_{MgO} between basins and through time reflects differences in the occurrence of carbonate minerals.

TiO₂ and Nb. Titanium and niobium have similar geochemical behaviour. These elements have a homogeneous distribution through time and in all the basins. The values of F_{TiO_2} and F_{Nb} show minor fluctuations and are generally close to or less than 1.

Fe₂O₃, MnO, Sc, V, Cr, Co, Ni, Cu and Zn. Fe₂O₃, MnO, and the transition trace elements (Sc, V, Cr, Co, Ni, Cu and Zn) yield enrichment factors that are generally below or close to 1, suggesting that the mafic supply from the provenance, for the time span considered, was negligible in the Guardia Pisano, Nurra, and Escalaplano basins (Fig. 8). However, notable exceptions, related to the enrichment of some elements, are observed in all the basins in both the Permian and Triassic samples. Fe₂O₃ is enriched only in two Triassic levels from the Escalaplano Basin (ET4 and ET5). In the Nurra Basin, the lower Permian sample NP2 is strongly enriched relative to the contiguous levels. MnO is strongly enriched in levels GPP3 and NP13, similar to that observed for CaO and MgO, suggesting that MnO may occur as carbonate. In NP13, minor enrichment is observed also for Sc and Co. Level NP4 is enriched in Ni, Cu, and Co. Two Triassic levels from the Escalaplano Basin are enriched in Cu (ET3 and ET7). Zn is enriched in the interval from ET3 to ET6.

Na₂O. Na₂O is depleted relative to the PAAS, yielding F_{Na_2O} values of <0.5, probably reflecting the paucity of feldspar. This may be due to either a high grade of maturity of the analyzed sediments or a feature peculiar to the source area(s).

K₂O, Rb, Cs. The K, Rb, and Cs contents in sediments are known to be associated with the detrital component (e.g., Plank and Langmuir, 1998). In the present case, the lack of feldspar means that K, Rb, and Cs are likely to be hosted by phyllosilicates. Although the distribution of K₂O, Rb, and Cs are very similar, the enrichment factors of Cs are, in many cases, significantly higher than those of K₂O and Rb. In the lowermost Permian samples from the Guardia Pisano Basin, F_{K_2O} and F_{Rb} are close to 1 whereas F_{Cs} ranging from 5 to 6. In the Nurra Basin, for both Permian and Triassic samples, F_{K_2O} , F_{Rb} , and F_{Cs} are all close to 1 with

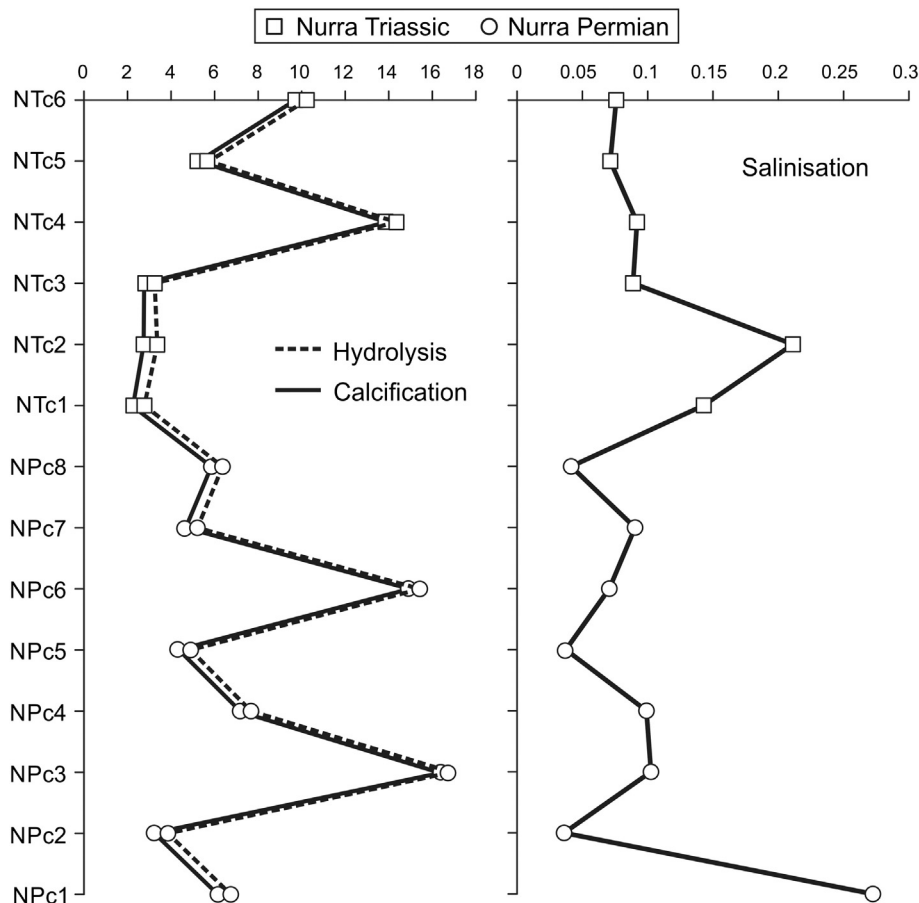


Fig. 5. Distribution of calcification, hydrolysis, and salinisation indexes through the Nurra succession. See text for further details.

the exception of F_{Cs} for the lower Permian samples of the Porto Ferro Formation, which have values higher than 3. F_{K_2O} and F_{Rb} are also close to 1 in the Triassic samples from the Escalaplano Basin, with the exception of the lowermost sample, which is enriched in both K and Rb. In this basin, Cs has an enrichment factor close to 1 for the ET1 and ET2 basal samples, whereas in the remaining part of the succession F_{Cs} is higher than 3. In general, the high values of F_{Cs} for some levels likely record changes in the detrital supply, since Cs is enriched during weathering relative to K and Rb (Perri et al., 2012).

Ba. Ba shows a different distribution from those of K_2O , Rb, Cs, with F_{Ba} generally being below 1. Barium is enriched in few samples, including the Guardia Pisano level GPP4 and especially the uppermost levels of the Permian sequence of the Nurra Basin (NP11, NP12, and NP13). These cases of Ba enrichment are probably related to the neoformation of authigenic barite, a well-documented process occurring in soils and continental deposits (Lynn et al., 1971; Stoops and Zavaleta, 1978; Podwojewski, 1995), including in the Sardinian domain (Mongelli et al., 2012).

P_2O_5 . Phosphorous exhibits different distributions in each of the three studied basins. In the lowermost Permian samples from the Guardia Pisano Basin, P_2O_5 is either close to 1 or is moderately enriched. In the Nurra Basin, $F_{P_2O_5}$ is below 1 with the exception of three lower Permian levels in which phosphorous is strongly enriched (NPT3, NP4, and NP5). In the Triassic Escalaplano Basin, phosphorous is moderately enriched and is only depleted in the uppermost ET7 level. The lack of any significant correlation between P_2O_5 and CaO ($r = -0.06$) and between P_2O_5 and La ($r = 0.05$) excludes the possibility that phosphorous fluctuations are simply due to fluctuations in the supply of apatite and monazite; rather, they may be related to palaeoenvironmental changes possibly driven by bacterial degradation of organic matter promoting precipitation of phosphatic phases (Mongelli et al., 2012 and references therein).

Pb. The distribution of Pb is similar to those of K_2O , Rb, and Cs both in the Guardia Pisano Basin, where F_{Pb} is above 1 with a maximum in the GPP3 level, and in the Nurra Basin, where F_{Pb} is generally less than 1 with the exceptions of the Permian levels NP3, NP4, and NP5. In contrast to K_2O , Rb, and Cs, Pb is depleted relative to PAAS in the Escalaplano Basin samples, with the exception of the uppermost level. It should be noted that, in both the Guardia Pisano Basin and Escalaplano Basin, the distribution of Pb mimics that of CaO, suggesting that lead may be hosted in the carbonate fraction. In contrast, the distribution of F_{Pb} in the Nurra Basin is very similar to that of $F_{P_2O_5}$ as reflected in the significant positive correlation between the Pb and P_2O_5 contents ($r = 0.82$), suggesting that the Pb distribution is principally controlled by the precipitation of phosphatic phases in this basin.

High field strength elements. A general increase in F_{Zr} and F_{Hf} values is observed from the bottom to the top levels for the Guardia Pisano Basin samples. The F_{Th} value shows negligible fluctuations and is close to 1. F_{Th} shows a similar trend in the Nurra Basin samples, with the exception of the uppermost Triassic level (NT2). F_{Zr} and F_{Hf} are both close to 1 in the lower Permian levels of the Nurra Basin, whereas the values increase in the upper Permian levels, reaching the maximum values in the NT2 sample. In the Triassic levels of the Escalaplano Basin, F_{Zr} , F_{Hf} , and F_{Th} values are either close to or below 1, and only in the uppermost level, ET7, show a moderate enrichment of high field strength elements (HFSEs) observed. The distribution of HFSEs is mainly controlled by minerals (e.g., zircon and monazite) that are concentrated in resistates during sedimentary processes. Thus, an increase in the enrichment factors for Zr, Hf, and Th may indicate relatively intense palaeoweathering conditions.

U. The values of F_U , F_{Zr} and F_{Hf} are similar in samples of the Nurra and Escalaplano basins, also to that of F_{Th} , suggesting that most of the uranium is associated with the resistates (see Table 4). The only notable exception is for the lower Permian level NP2 in the Nurra Basin, in which F_U has a value of 3.2, whereas F_{Zr} , F_{Hf} , and F_{Th} show values below 1. The behaviour of U in the sedimentary environment depends

on redox conditions and, in oxidizing environments, U is soluble as U^{6+} (Takeno, 2005); therefore, the high value of F_U in NP2 may reflect precipitation of U under more reducing conditions.

REEs and Y. In the Guardia Pisano Basin, REE and Y show enrichment factors close to 1, with the exception of level GPP3 in which the enrichment factors lie in the range of 1.5–2.5 (Fig. 9). In the lower Permian samples NP2 and NP4 from the Nurra Basin, LREEs and medium REEs (MREEs) show enrichment factors ranging from 1.6 to 2.8 (Fig. 9). In the other Permian levels, the REEs and Y are generally moderately enriched and increases in the enrichment factors are observed only in the uppermost Permian levels and the Triassic levels, especially for HREEs. In the Triassic Escalaplano Basin, the enrichment factors are generally close to 1, and depletion in LREEs and MREEs is observed in the uppermost part of the sequence (Fig. 9).

The LREEs and HREEs distributions vary along the stratigraphic successions, as shown by $(La/Yb)_N$ index. In the Guardia Pisano Basin, the $(La/Yb)_N$ fractionation index is lower than that of PAAS ($(La/Yb)_N = 9.2$). Exceptions to this trend are observed in the Nurra Basin for Permian levels NP2 and NP4. Notably, the uppermost Triassic level NP13 of the Nurra Basin shows a very low $(La/Yb)_N$ index. In the Triassic Escalaplano Basin, $(La/Yb)_N$ exceeds 9.2 for several levels (Table 3). However, overall, the REE chondrite-normalised patterns are PAAS-like (Fig. 10). The average Eu anomalies for the three studied basins are similar or slightly lower than that of PAAS ($Eu/Eu^* = 0.66$). Finally, it should be noted that high carbonate and quartz abundances dilute REE contents, and levels with lower total REE (ΣREE) contents are high in either CaO (GPP3, ET2, ET7) or SiO_2 (NP2, NP3, NP5) contents (Table 3).

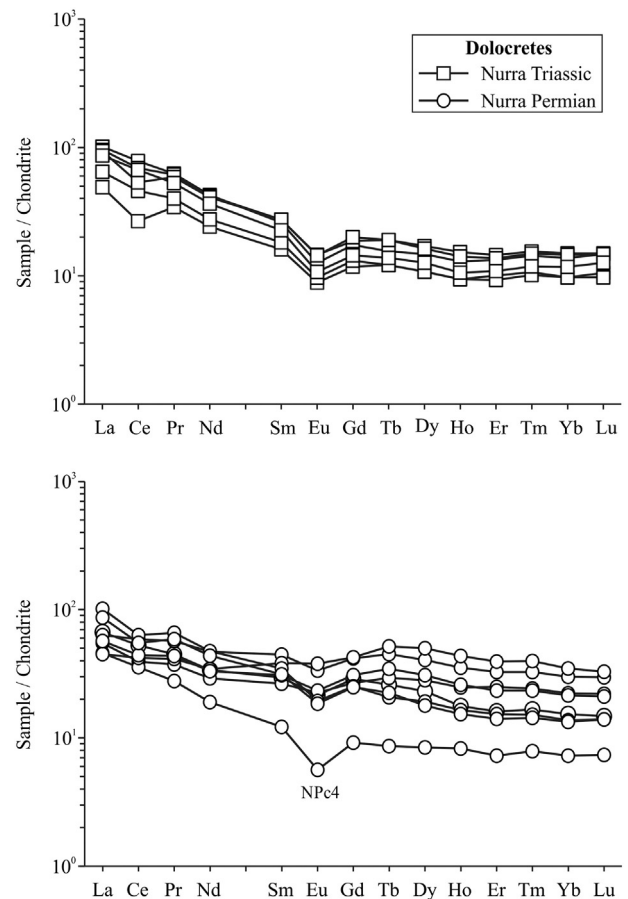


Fig. 6. Chondrite-normalised rare earth element (REE) patterns of Nurra dolocretes; chondrite values are from Evensen et al. (1978).

Table 4
Enrichment factors for selected elements of the shales.

Elements	Nurra Basin samples															Min.	Max.	Mean	σ
	NT2	NT1	NP13	NP12	NP11	NP10	NP9	NP8	NP7	NP6	NP5	NP4	NP3	NP2	NP1				
<i>Major elements</i>																			
FSiO ₂	1.73	1.04	1.78	1.56	1.11	1.27	1.42	0.96	0.99	1.01	2.20	1.59	2.84	4.24	0.88	0.88	4.24	1.6	0.9
FFe ₂ O ₃	0.91	1.09	0.76	0.62	1.12	0.90	0.85	1.13	1.13	1.05	0.14	0.32	0.17	0.89	0.07	0.07	1.13	0.7	0.4
FMnO	0.72	0.74	4.28	1.57	0.65	0.16	0.98	0.31	0.26	0.21	0.09	0.18	0.19	1.24	0.89	0.09	4.28	0.8	1.1
FMgO	1.37	1.76	4.13	1.66	0.94	0.54	1.21	0.58	0.58	0.49	0.26	0.27	0.28	0.23	0.12	0.12	4.13	1.0	1.0
FCaO	2.36	3.19	11.52	4.26	1.15	0.09	2.49	0.29	0.31	0.11	0.38	0.51	0.31	0.16	0.20	0.09	11.52	1.8	3.0
FNa ₂ O	0.33	0.24	0.21	0.20	0.17	0.15	0.18	0.17	0.44	0.15	0.14	0.11	0.19	0.25	0.13	0.11	0.44	0.2	0.1
FK ₂ O	1.54	1.62	1.45	1.49	1.58	1.18	1.42	1.42	1.37	1.33	1.26	1.25	1.37	1.09	0.62	0.62	1.62	1.3	0.2
FTiO ₂	1.18	0.94	0.85	0.93	0.90	0.94	0.81	0.76	0.82	0.76	0.75	0.74	0.71	0.60	0.91	0.60	1.18	0.8	0.1
FP ₂ O ₅	0.69	1.05	0.48	0.57	0.57	0.15	0.50	0.81	0.45	0.32	2.32	3.49	1.84	0.75	1.34	0.15	3.49	1.0	0.9
<i>Trace elements</i>																			
FCr	0.58	0.66	0.35	0.55	0.63	0.64	0.61	0.63	0.66	0.56	0.92	0.85	0.77	0.55	1.09	0.35	1.09	0.7	0.2
FV	0.65	0.69	0.66	0.67	0.79	0.67	0.63	0.72	0.72	0.61	0.79	0.84	0.80	1.01	0.48	0.48	1.01	0.7	0.1
FSc	1.09	1.05	1.45	0.85	0.93	0.88	0.93	0.99	1.03	0.83	0.74	1.00	0.92	0.94	0.37	0.37	1.45	0.9	0.2
FCo	0.34	0.47	1.34	0.73	0.40	0.36	0.64	0.39	0.54	0.36	0.44	1.39	0.27	0.39	0.30	0.27	1.39	0.6	0.4
FNi	0.60	0.59	0.84	0.66	0.69	0.45	0.59	0.70	0.67	0.60	0.52	1.26	0.50	0.71	0.61	0.45	1.26	0.7	0.2
FZn	0.39	0.38	0.52	0.43	0.55	0.48	0.54	0.82	0.97	0.78	0.54	0.42	0.40	0.25	0.09	0.09	0.97	0.5	0.2
FCu	0.22	0.12	0.39	0.36	0.30	0.44	0.51	0.30	0.25	0.27	1.08	1.41	0.67	0.36	0.38	0.12	1.41	0.5	0.3
FCs	1.27	1.73	1.35	1.83	2.62	2.07	1.81	3.91	4.10	3.41	1.57	1.28	1.59	1.33	0.61	0.61	4.10	2.0	1.0
FBa	0.57	0.69	10.21	8.34	2.37	0.66	1.15	0.65	0.63	0.63	0.66	0.54	0.70	0.74	0.28	0.28	10.21	1.9	3.0
FRb	1.21	1.36	0.99	1.17	1.40	1.24	1.19	1.55	1.47	1.39	1.28	1.21	1.25	1.06	0.52	0.52	1.55	1.2	0.2
FSr	1.09	1.00	0.97	0.94	0.83	0.35	0.51	0.73	0.62	0.58	0.63	0.79	0.59	0.82	0.37	0.35	1.09	0.7	0.2
FPb	0.63	0.42	0.24	0.19	0.92	0.76	0.67	1.24	1.24	0.87	5.56	6.45	2.84	0.38	0.26	0.19	6.45	1.5	1.9
FY	1.93	1.34	2.07	1.69	1.32	1.17	1.40	1.25	1.15	1.10	1.31	1.72	1.17	1.23	1.30	1.10	2.07	1.4	0.3
FTh	1.91	1.38	1.44	1.64	1.21	1.51	1.35	1.26	1.16	1.23	1.21	1.22	1.12	0.97	1.09	0.97	1.91	1.3	0.2
FU	2.60	1.59	2.18	2.10	1.48	1.96	1.78	1.03	1.03	1.06	1.41	1.24	1.22	3.21	1.08	1.03	3.21	1.7	0.6
FZr	3.05	1.38	1.68	2.20	1.18	1.94	1.69	0.73	0.86	1.03	0.88	0.87	0.77	0.73	0.91	0.73	3.05	1.3	0.7
FHF	3.10	1.52	1.70	2.24	1.24	2.01	1.83	0.83	0.93	1.17	0.84	0.90	0.76	0.66	1.01	0.66	3.10	1.4	0.7
FNb	1.25	1.08	0.81	0.88	1.03	0.92	0.78	0.99	0.98	0.92	0.71	0.70	0.55	0.48	0.72	0.48	1.25	0.9	0.2
<i>Rare earth elements</i>																			
FLa	2.03	1.54	1.17	1.73	1.34	1.40	1.47	1.26	1.11	1.17	1.17	1.73	1.02	1.92	0.93	0.93	2.03	1.4	0.3
FCe	1.90	1.32	1.11	1.69	1.28	1.31	1.38	1.23	1.05	1.09	1.07	1.70	0.95	1.62	0.86	0.86	1.90	1.3	0.3
FPr	1.96	1.38	1.17	1.69	1.26	1.30	1.42	1.23	1.02	1.06	1.12	1.79	0.97	1.60	0.92	0.92	1.96	1.3	0.3
FNd	1.90	1.31	1.20	1.64	1.23	1.23	1.38	1.17	0.97	1.03	1.12	1.86	0.97	1.66	0.96	0.96	1.90	1.3	0.3
FSm	2.06	1.48	1.69	1.84	1.35	1.34	1.59	1.38	1.07	1.12	1.29	2.33	1.24	1.67	1.13	1.07	2.33	1.5	0.4
FEu	1.68	1.45	1.68	1.45	1.20	1.00	1.28	1.34	0.99	1.00	1.46	2.64	1.36	1.81	1.26	0.99	2.64	1.4	0.4
FGd	1.99	1.51	2.14	2.00	1.34	1.20	1.55	1.29	1.03	1.00	1.54	2.77	1.39	1.61	1.40	1.00	2.77	1.6	0.5
FTb	2.26	1.72	2.51	1.97	1.34	1.37	1.57	1.42	1.20	1.06	1.75	2.76	1.37	1.57	1.45	1.06	2.76	1.7	0.5
FDy	2.16	1.70	2.59	2.07	1.43	1.41	1.71	1.40	1.31	1.21	1.57	2.48	1.44	1.37	1.50	1.21	2.59	1.7	0.4
FHo	1.90	1.45	2.12	1.82	1.26	1.29	1.48	1.29	1.13	1.13	1.35	1.86	1.26	1.21	1.29	1.13	2.12	1.5	0.3
FEr	1.96	1.41	1.93	1.78	1.26	1.29	1.49	1.27	1.14	1.17	1.28	1.65	1.16	1.35	1.24	1.14	1.96	1.4	0.3
FTm	2.18	1.69	2.17	1.93	1.43	1.49	1.68	1.37	1.29	1.28	1.35	1.63	1.26	1.43	1.31	1.26	2.18	1.6	0.3
FYb	2.09	1.51	2.07	1.79	1.39	1.46	1.59	1.28	1.21	1.24	1.26	1.38	1.20	1.40	1.19	1.19	2.09	1.5	0.3
FLu	2.21	1.54	2.16	1.94	1.41	1.55	1.66	1.34	1.27	1.31	1.33	1.36	1.22	1.40	1.22	1.22	2.21	1.5	0.3

Elements	Escalaplano Basin samples											Guardia Pisano Basin samples									
	ET7	ET6	ET5	ET4	ET3	ET2	ET1	Min.	Max.	Mean	σ	GPP5	GPP4	GPP3	GPP2	GPP1	Min.	Max.	Mean	σ	
<i>Major elements</i>																					
FSiO ₂	1.20	0.79	1.05	0.91	0.97	0.82	0.84	0.79	1.20	0.9	0.1	1.47	1.62	2.08	0.96	1.03	0.96	2.08	1.4	0.5	
FFe ₂ O ₃	0.54	1.25	1.80	1.78	0.99	0.94	0.96	0.54	1.80	1.2	0.5	1.21	1.30	1.31	0.90	0.81	0.81	1.31	1.1	0.2	
FMnO	0.27	0.72	0.75	0.73	0.55	0.59	0.95	0.27	0.95	0.7	0.2	0.92	0.95	2.78	0.46	0.33	0.33	2.78	1.1	1.0	
FMgO	3.95	2.95	2.68	3.08	3.10	1.65	1.67	1.65	3.95	2.7	0.8	0.58	0.58	0.58	1.33	0.65	0.58	1.33	0.7	0.3	
FCaO	10.04	1.51	5.73	3.72	2.80	4.30	6.00	1.51	10.04	4.9	2.8	8.97	8.02	14.95	3.35	2.47	2.47	14.95	7.6	5.0	
FNa ₂ O	0.17	0.20	0.26	0.22	0.25	0.12	0.21	0.12	0.26	0.2	0.0	0.45	0.28	0.38	0.25	0.19	0.19	0.45	0.3	0.1	
FK ₂ O	2.95	1.53	1.56	1.60	1.61	1.25	1.21	1.21	2.95	1.7	0.6	1.01	1.01	0.98	1.03	0.84	0.84	1.03	1.0	0.1	
FTiO ₂	0.31	0.75	0.85	0.81	0.83	0.55	0.59	0.31	0.85	0.7	0.2	0.96	1.01	1.01	0.68	0.65	0.65	1.01	0.9	0.2	
FP ₂ O ₅	0.49	1.37	1.44	1.55	1.49	1.88	1.60	0.49	1.88	1.4	0.4	1.05	1.20	1.30	1.36	0.86	0.86	1.36	1.2	0.2	
FCr	0.14	0.76	0.86	0.79	0.76	0.66	0.78	0.14	0.86	0.7	0.2	0.70	0.58	0.76	0.50	0.48	0.48	0.76	0.6	0.1	
FV	0.32	0.92	1.06	1.07	1.00	1.05	0.86	0.32	1.07	0.9	0.3	1.00	0.91	0.91	0.71	0.64	0.64	1.00	0.8	0.2	
FSc	1.18	1.04	1.10	1.09	1.12	1.17	1.14	1.04	1.18	1.1	0.0	1.05	1.10	1.17	0.95	0.80	0.80	1.17	1.0	0.1	
FCo	0.14	0.86	0.94	0.81	1.14	0.63	0.70	0.14	1.14	0.7	0.3	0.53	0.56	0.63	0.71	0.42	0.42	0.71	0.6	0.1	
FNi	0.17	0.91	0.91	0.86	0.98	0.60	0.72	0.17	0.98	0.7	0.3	0.78	0.82	0.94	0.77	0.56	0.56	0.94	0.8	0.1	
FZn	0.46	1.69	1.77	1.64	1.79	1.15	1.32	0.46	1.79	1.4	0.5	1.40	1.45	1.56	1.65	1.24	1.24	1.65	1.5	0.2	
FCu	2.19	0.38	0.30	0.27	2.51	0.37	1.09	0.27	2.51	1.0	1.0	0.58	0.67	0.96	0.57	0.38	0.38	0.96	0.6	0.2	
FCs	3.09	3.26	3.13	3.44	3.00	1.20	1.26	1.20	3.44	2.6	1.0	5.24	5.60	5.30	5.83	5.78	5.24	5.83	5.6	0.3	
FBa	0.53	0.88	1.00	0.88	0.90	0.94	1.04	0.53	1.04	0.9	0.2	0.85	1.29	0.94	0.74	0.78	0.74	1.29	0.9	0.2	
FRb	1.68	1.45	1.40	1.40	1.40	1.35	1.32	1.32	1.68	1.4	0.1	1.08	1.09	1.04	1.21	1.05	1.04	1.21	1.1	0.1	
FSr	0.28	0.38	0.49	0.88	2.06	0.93	1.63	0.28	2.06	1.0	0.7	0.93	0.95	1.06	2.34	1.37	0.93	2.34	1.3	0.6	
FPb	1.02	0.13	0.61	0.50	0.42	0.42	0.13	0.13	1.02	0.5	0.3	1.53	1.68	2.70	1.91	1.70	1.53	2.70	1.9	0.5	
FY	0.58	0.89	1.05	0.97	0.97	0.73	0.79	0.58	1.05	0.9	0.2	1.42	1.43	1.92	1.29	1.26	1.26	1.92	1.5	0.3	
FTh	1.57	0.94	1.03	0.98	1.05	0.82	0.78	0.78	1.57	1.0	0.3	1.10	1.16	1.25	1.31	1.32	1.10	1.32	1.2	0.1	
FU	1.57	1.01	1.40	1.48	1.50	0.94	1.03	0.94	1.57	1.3	0.3	1.14	1.14	1.27	0.84	0.55	0.55	1.27	1.0	0.3	
FZr	1.08	0.54	0.75	0.67	0.72	0.46	0.45	0.45	1.08	0.7	0.2	1.34	1.57	1.90	0.62	0.67	0.62	1.90	1.2	0.6	
FHF	1.47	0.56	0.76	0.69	0.77	0.50	0.49	0.49	1.47	0.7	0.3	1.41	1.57	2.04	0.70	0.77	0.70	2.04	1.3	0.6	
FNb	0.49	0.66	0.64	0.65	0.69	0.38	0.51	0.38	0.69	0.6	0.1	0.97	1.01	0.98	0.80	0.84	0.80	1.01	0.9	0.1	
<i>Rare earth elements</i>																					
FLa	0.59	0.96	1.20	1.14	1.11	0.76	0.70	0.59	1.20	0.9	0.2	1.28	1.32	1.51	0.92	0.98	0.92	1.51	1.2	0.2	
FCe	0.62	0.94	1.15	1.08	1.06	0.72	0.66	0.62	1.15	0.9	0.2	1.21	1.25	1.50	1.01	0.99	0.99	1.50	1.2	0.2	
FPr	0.57	0.94	1.12	1.05	1.09	0.74	0.67	0.57	1.12	0.9	0.2	1.24	1.25	1.52	1.06	0.97	0.97	1.52	1.2	0.2	
FNd	0.57	0.99	1.17	1.10	1.13	0.81	0.73	0.57	1.17	0.9	0.2	1.22	1.23	1.54	1.10	0.98	0.98	1.54	1.2	0.2	
FSm	0.62	1.16	1.28	1.24	1.26	0.96	0.88	0.62	1.28	1.1	0.2	1.45	1.40	1.89	1.44	1.14	1.14	1.89	1.5	0.3	
FEu	0.44	1.17	1.26	1.30	1.21	0.90	0.86	0.44	1.30	1.0	0.3	1.39	1.34	1.96	1.22	0.91	0.91	1.96	1.4	0.4	
FGd	0.57	1.07	1.27	1.19	1.20	0.95	0.93	0.57	1.27	1.0	0.2	1.50	1.47	2.12	1.53	1.20	1.20	2.12	1.6	0.3	
FTb	0.61	1.08	1.23	1.13	1.24	0.94	0.97	0.61	1.24	1.0	0.2	1.59	1.67	2.43	1.70	1.38	1.38	2.43	1.8	0.4	
FDy	0.71	1.00	1.20	1.13	1.22	0.90	0.95	0.71	1.22	1.0	0.2	1.70	1.68	2.27	1.63	1.40	1.40	2.27	1.7	0.3	
FHo	0.63	0.83	1.08	0.99	1.08	0.83	0.85	0.63	1.08	0.9	0.2	1.53	1.44	1.87	1.31	1.28	1.28	1.87	1.5	0.2	
FEr	0.70	0.83	1.03	0.94	0.99	0.79	0.77	0.70	1.03	0.9	0.1	1.42	1.38	1.86	1.28	1.21	1.21	1.86	1.4	0.3	
FTm	0.86	0.97	1.18	1.12	1.14	0.88	0.91	0.86	1.18	1.0	0.1	1.53	1.56	1.97	1.39	1.36	1.36	1.97	1.6	0.2	
FYb	0.90	0.86	1.11	1.02	1.07	0.85	0.92	0.85	1.11	1.0	0.1	1.42	1.43	1.85	1.32	1.25	1.25	1.85	1.5	0.2	
FLu	0.91	0.92	1.10	1.10	1.08	0.89	0.89	0.89	1.10	1.0	0.1	1.46	1.57	1.98	1.32	1.31	1.31	1.98	1.5	0.3	

Min., Max., Mean, and σ refer to the minimum, maximum, mean, and standard deviation values respectively.

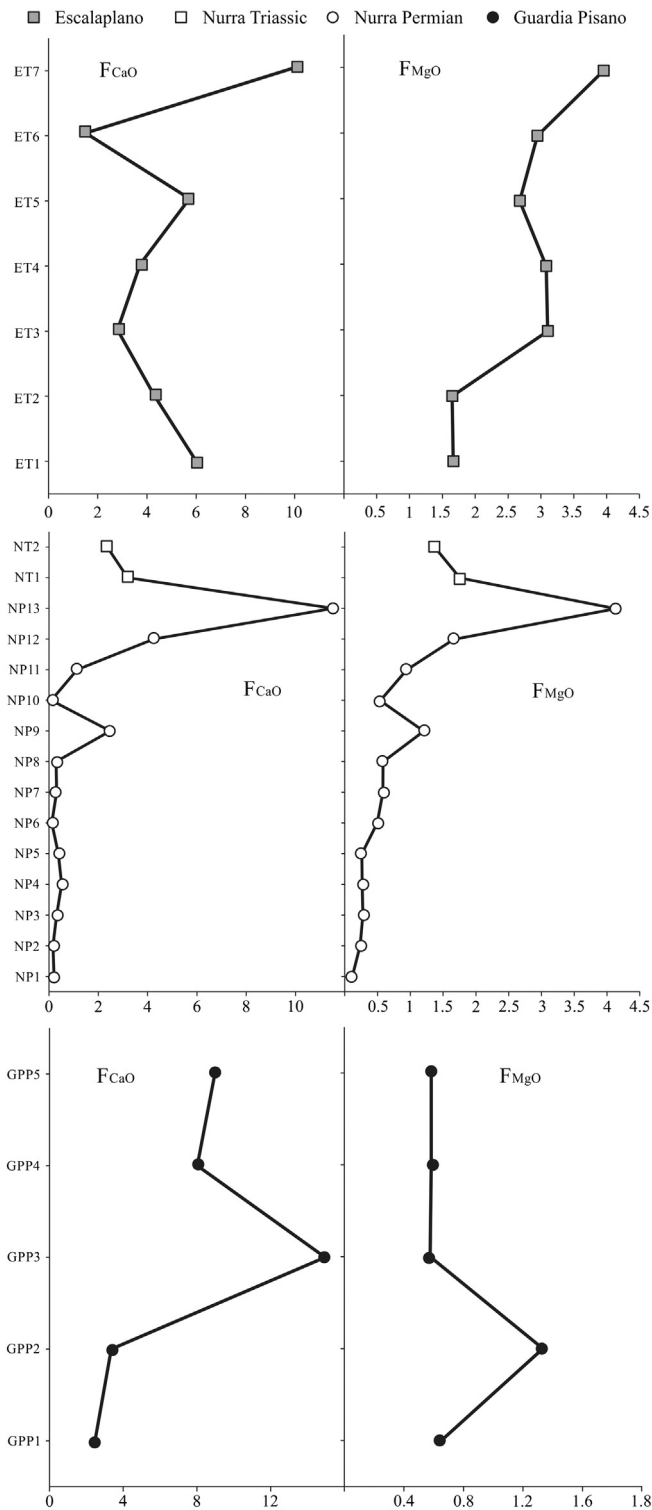


Fig. 7. Enrichment factors for CaO and MgO in the Permian and Triassic samples of Escalaplano, Nurra, and Guardia Pisano basins.

5. Discussion

The chemical composition of fine-grained siliciclastic sediments, including those forming continental successions such as red beds, is known to be affected by several factors including provenance, source-area weathering, sorting and recycling, and post-depositional reactions (Perri et al., 2012). Furthermore, in continental successions, palaeoclimatic changes are often recorded by carbonate-rich palaeosols,

to which relatively little attention has been paid (e.g., Basilici et al., 2009). Thus, we discuss our data for both dolocretes and siliciclastic sediments to obtain a more comprehensive picture of the Permian–Triassic evolution of the Sardinia domain.

5.1. Dolocretes

The precipitation of carbonate in soils is a complex phenomenon, and many models have been developed to describe its formation in different environments (e.g., Mikhailova and Post, 2006). In our geological scenario, the most likely model appears to be the “per ascensum model”, which involves carbonate formation associated with a capillary rise of Ca^{2+} , Mg^{2+} , and bicarbonate from a shallow water table and subsequent precipitation of carbonates in soil under a dry climate (Sobecki and Wilding, 1983; Alonso-Zarza et al., 2009). In the Nurra Basin, the siliciclastic sediments are often coupled with an accumulation of pedogenic carbonate. In drier conditions, Ca^{2+} and Mg^{2+} are less readily leached from soils and accumulate as carbonate minerals. The observed variation in the calcification index, along with the very high values of this ratio observed in some samples, suggests that decidedly arid conditions were not rare, consistent with the hypothesis that Permian and Triassic climates were semiarid (with strong seasonality) to arid (e.g., Gómez-Gras and Alonso-Zarza, 2003). In addition, the values of the base/alumina ratio are consistently greater than 1, which reflects an alkaline-evolved soil that, coupled with the absence of siderite and calcium sulphate, hosted carbonate precipitated from fluid with a pH of 8.0–8.5 (Retallack, 2001). Finally, the salinisation ratio, which is always lower than 1, supports the idea of carbonate precipitation from shallow groundwater. Overall, these features point towards low-sinuosity river systems with thick floodplain deposits under arid or semiarid conditions (De la Horra et al., 2012).

5.2. Siliciclastic sediments

5.2.1. Source-area weathering

The relationship between mobile and immobile elements was used to reconstruct the weathering conditions affecting the source rocks. Several indices have been utilised in the literature as broad measures of palaeoweathering. Among them, the Chemical Index of Alteration (CIA; Nesbitt and Young, 1982; $\text{CIA} = [\text{Al}_2\text{O}_3 / (\text{Al}_2\text{O}_3 + \text{CaO}^* + \text{Na}_2\text{O} + \text{K}_2\text{O})] \cdot 100$, where the elements are in molecular proportions and CaO^* is the amount of CaO residing in silicate minerals only) is considered the most reliable palaeoweathering proxy, although caution is due when K-metasomatism occurs (Roy and Roser, 2013). Alternatively, the Chemical Index of Weathering (CIW; Harnois, 1988; $\text{CIW} = [\text{Al}_2\text{O}_3 / (\text{Al}_2\text{O}_3 + \text{CaO}^* + \text{Na}_2\text{O})] \cdot 100$), which is not sensitive to postdepositional K-enrichment, provides reliable information about source-area weathering (e.g., Mongelli et al., 2006). These proxies are based on the assumption that the leaching of alkalis (Na^+ and K^+) and Ca^{2+} , and the concentration of Al and Si in the residue are the dominant processes during chemical alteration of the protolith allowing the degradation of feldspars and the formation of clay minerals. Unweathered igneous rocks have CIA values of 50 or less, residual clays have values close to 100, and the PAAS has an average CIA value of 67 (McLennan et al., 1993) and an average CIW value of 85. In addition, the distribution of REEs in sediments may yield insights concerning weathering in the source area because intense weathering produces LREE/HREE fractionation although REEs are preferentially transferred from the source to the sediment (e.g., Mongelli, 2004; Mongelli et al., 2006, and references therein). In siliciclastic sediments, this is recognised by the variation of the $(\text{La}/\text{Yb})_N$ ratio through a succession (e.g., Mongelli et al., 2006), and ratio distributions may differ among basins.

Overall, the samples of Sardinian red beds, despite their variation in age, are generally characterised by average CIA values of less than 74

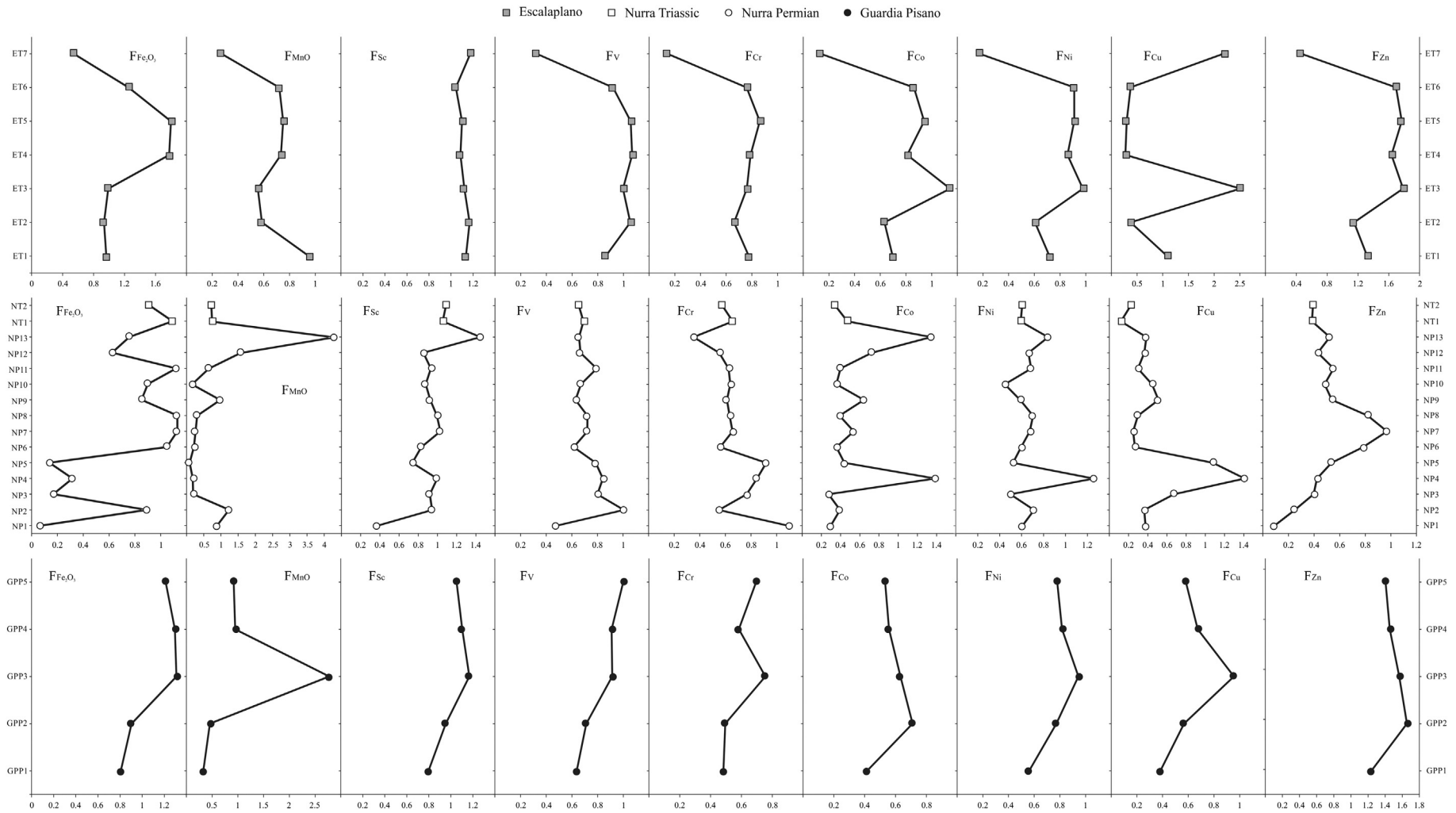


Fig. 8. Distribution of enrichment factors for Fe_2O_3 , MnO, and transition trace elements through the Escalaplano, Nurra, and Guardia Pisano successions. See text for further details.

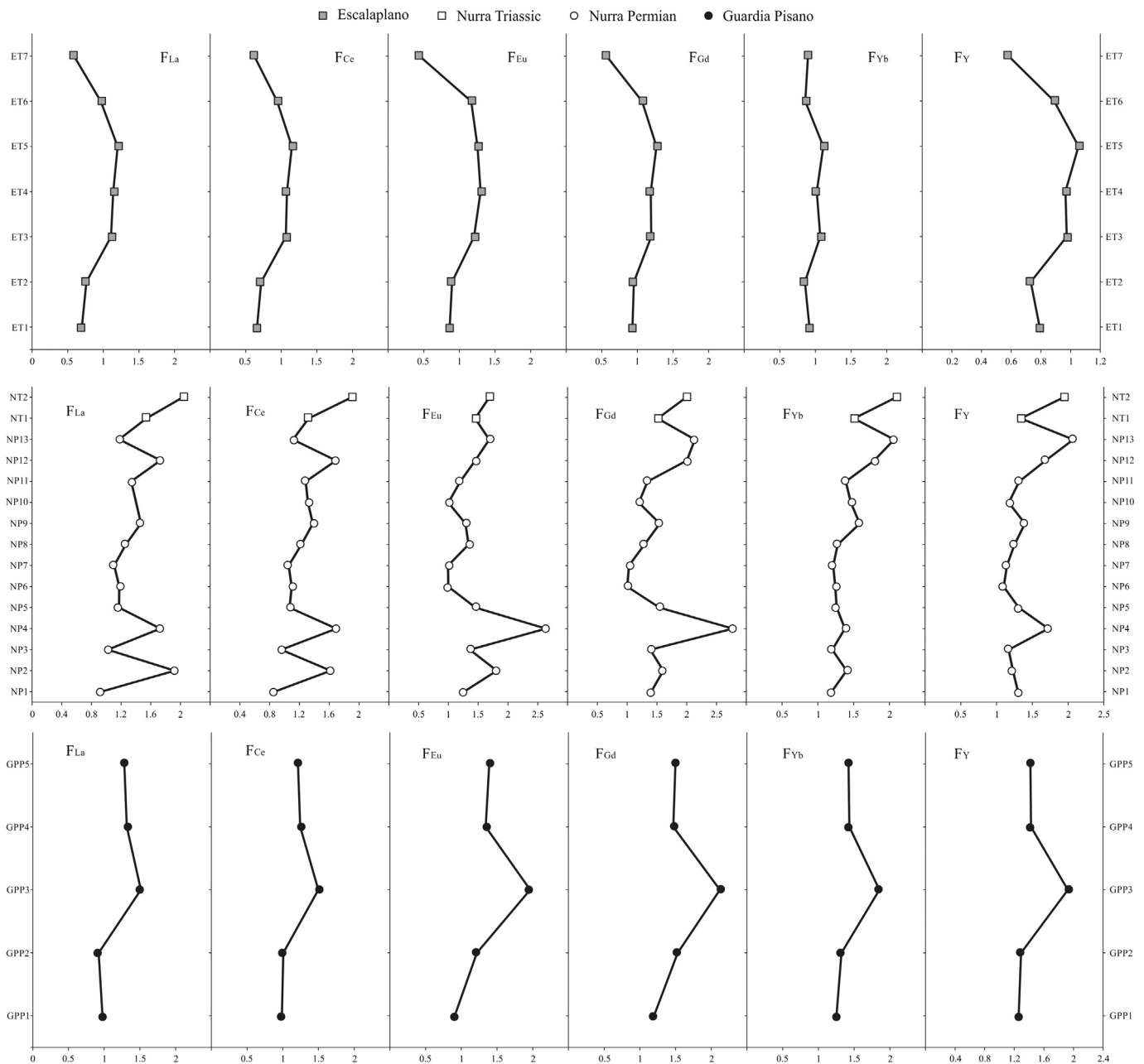


Fig. 9. Enrichment factors for selected rare earth elements and Y in the Permian and Triassic samples of Escalaplano, Nurra, and Guardia Pisano basins.

(excluding sample NP1 with a value of 82), testifying to a moderate degree of source-area weathering. Weathering trends can be illustrated on an A-CN-K triangular diagram (Fig. 11) where the vertical dimension ($A = \% \text{Al}_2\text{O}_3$) corresponds to values of CIA (Nesbitt and Young, 1984, 1989). In the lower Permian samples from the Guardia Pisano Basin, the trend is parallel to the A-CN join, towards the 2:1 phyllosilicates, and both the CIA (average $\text{CIA} = 67 \pm 4$) and CIW (average $\text{CIW} = 84 \pm 5$) values are close to those typical for shales formed through moderate weathering in the source area. In addition, the $(\text{La}/\text{Yb})_N$ index (average $(\text{La}/\text{Yb})_N = 7.5 \pm 0.8$) is quite lower than that for PAAS ($(\text{La}/\text{Yb})_N = 9.2$), thus confirming the patterns exhibited by the CIA and CIW proxies. The Permian samples from the Nurra Basin, are characterised by CIA values typical of shales formed through moderate weathering in the source area (average $\text{CIA} = 69 \pm 5$) although show a wide dispersion. However, in the A-CN-K diagram, most of the samples fall close to the A-K join towards the K apex, suggesting the addition of diagenetic potassium (e.g., Perri et al., 2011, and references

therein). In the present case, the CIW proxy is the more reliable palaeoweathering recorder, since the CIA index is insensitive to the degree of weathering when K reintroduction occurs in the system. The Nurra Basin samples yield homogeneous CIW values (average $\text{CIW} = 95 \pm 4$), indicating intense weathering in the source area. More intense weathering conditions in the source area are also indicated by the values of the LREE/HREE ratio, which are higher for the Nurra Permian samples (average $(\text{La}/\text{Yb})_N = 8.8 \pm 1.8$) than those of the Guardia Pisano Basin. In this scenario, the regional relevance of the Variscan relief must be emphasised, including that of the Sardinia-Corsica Variscides, which was characterised by high relief in the range of 2000–4000 m during the Permian (Fluteau et al., 2001). This relief could have fostered more humid conditions related to orographic and windward-side rainfall, which in turn enhanced weathering in the source area(s) of proximal basins such as the Nurra Basin (Fig. 12). The estimated degree of palaeoweathering in the source area for the Nurra Basin samples is also consistent with the growing consensus

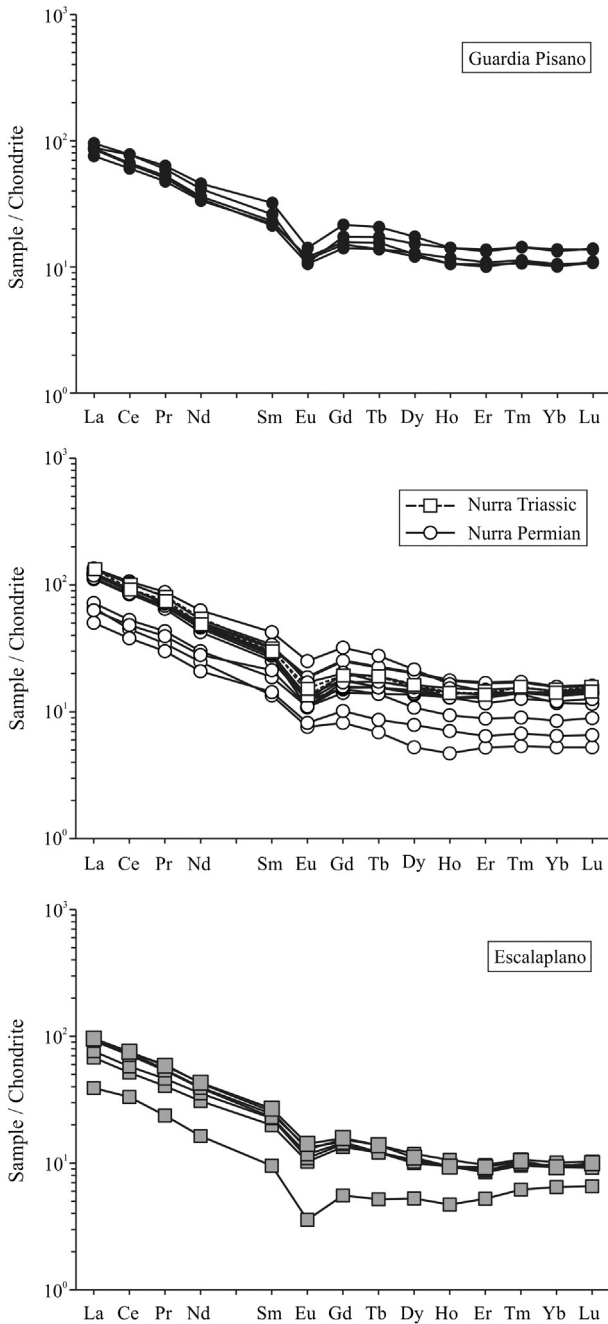


Fig. 10. Chondrite-normalised REE patterns of studied siliciclastic sediments; chondrite values are from Evensen et al. (1978).

about the global switch to a more humid climate at the end of the middle Permian, which was characterised by enhanced chemical weathering (De la Horra et al., 2012 and references therein). The diagenetic K-metasomatism affecting the Nurra Permian samples implies that the Nurra Basin experienced a degree of burial due to lithostatic loading. In fact, the thickness of the Mesozoic cover (mostly carbonates) above the Triassic red beds generally exceeds 1 km. This phenomenon is widespread in ancient red beds from the Mediterranean domain due to its complex tectonic evolution (e.g., Perri et al., 2011, 2013 and references therein), and such burial is not surprising given that the Nurra Basin is the largest and deepest intramontane basin of the Sardinia-Corsica fragment (Cassinis et al., 2003). Finally, the Triassic levels of the Escalaplano Basin have low CIA and CIW values (average CIA = 60 ± 4 , average CIW = 83 ± 6 ; level ET7 was excluded from the calculation likely due to high calcite contents causing an error in the evaluation of CaO*). The palaeoweathering proxies indicate that the source-area weathering for the sediments of the Escalaplano Basin is weak. However, the samples in the A-CN-K diagram broadly form an array parallel to the A-CN join (Fig. 11). Therefore, the weathering effect may be assumed as minor but not negligible, according to the (La/Yb)_N values (average (La/Yb)_N = 8.7 ± 1.7). However, the palaeoweathering proxies suggest that the climate in the source area was characterised by dry conditions.

5.2.2. Sorting and recycling

The transport and deposition of clastic sediments involves mechanical sorting. Its effect on the chemical composition of terrigenous sediments is important and may affect the distribution of palaeoweathering and provenance proxies (Mongelli et al., 2006; Perri et al., 2012). The distribution of the chemical components within a suite is determined mainly by the mechanical properties of the host minerals. The process fractionates Al₂O₃ (phyllosilicates) from SiO₂ (quartz and feldspars). Sorting also fractionates TiO₂, mostly present in clay minerals and Ti oxides, from Zr, present in zircon, and sorted with quartz. However, the variable content of inert elements in siliciclastic sediments is due mostly to the degree of weathering, which affects parent rocks (e.g., Perri et al., 2013). Ternary plots based on Al₂O₃, TiO₂, and Zr eliminate these weathering effects and may show the presence of sorting-related fractionations, which are recognisable by simple mixing trends on a ternary Al₂O₃-TiO₂-Zr diagram (Garcia et al., 1991). In the present case, a trend characterised mainly by changes in the Al₂O₃/Zr ratio, which could be due to a recycling effect, is clearly shown for the Guardia Pisano and the Nurra basins (Fig. 13).

Zircon, and thus Zr enrichment during sorting, can also be evaluated when the Zr/Sc ratio, a useful index of sediment recycling (e.g., Hassan et al., 1999), is plotted against the Th/Sc ratio, an indicator of chemical differentiation (McLennan et al., 1993). In this binary plot, most of the samples are not clustered along the primary compositional trend but

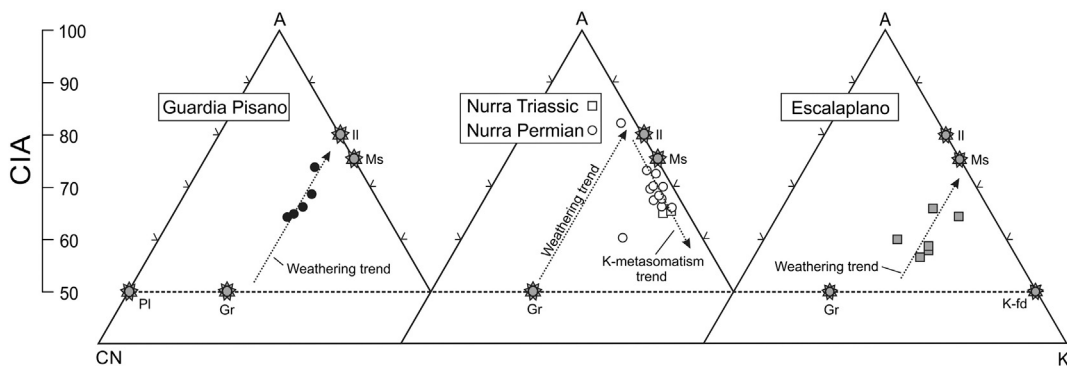


Fig. 11. A-CN-K diagram for studied red beds. Pl, plagioclase; Gr, granite; K-fd, K-feldspar; Ms, muscovite; Il, illite. The Guardia Pisano and Escalaplano sediments show a typical trend of moderate weathering; the Nurra samples, instead, fall close to the A-K join along a trend indicating K addition during diagenesis.

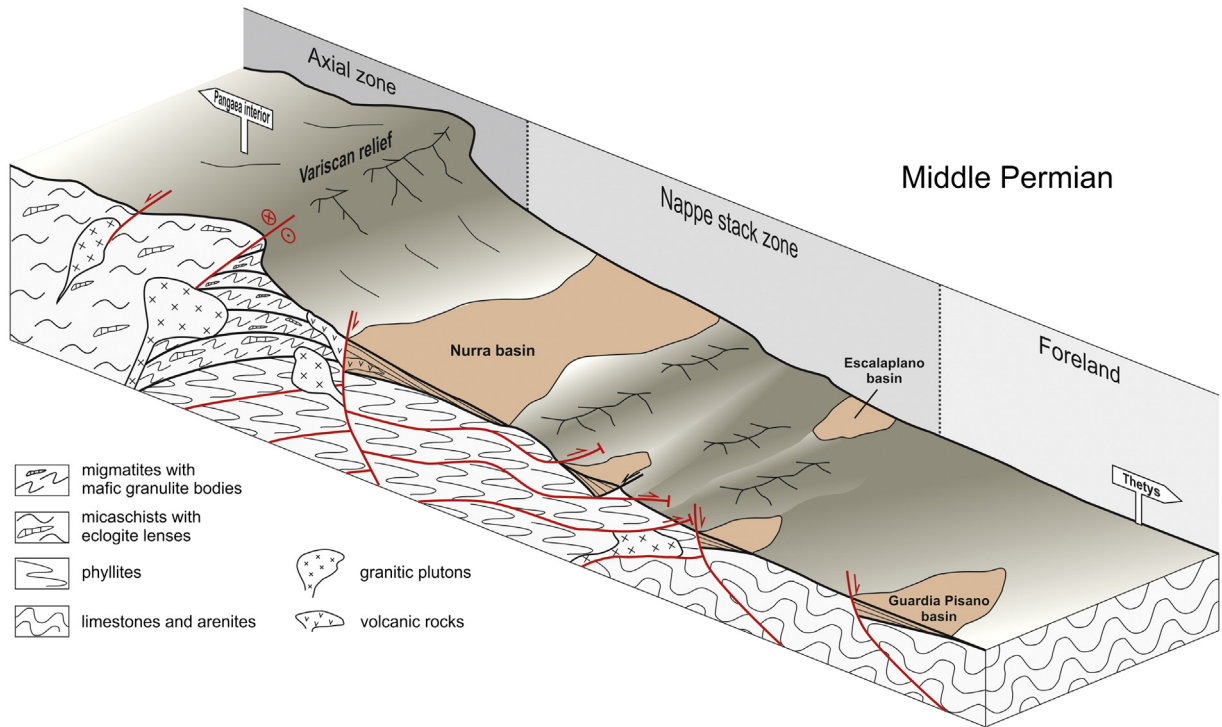


Fig. 12. Middle Permian alleged paleoenvironmental reconstruction from chain to foreland of a portion of the South European Variscan orogeny actually exposed in the Sardinia–Corsica microplate.

rather fall along a trend involving the addition of zircon (Fig. 14), thereby indicating sediment recycling, consistent with the Al_2O_3 – TiO_2 –Zr diagram. The samples most likely affected by recycling effects are those forming the upper part of the Guardia Pisano Basin (from GPP3 to GPP5), the part upper Permian in age of the Nurra succession (from NP9 to NP13), and the two Triassic samples from the Nurra succession.

Regarding the Nurra Basin samples, it should be noted that, in the northwestern peri-Tethyan domain, the variable pattern of palaeocurrent directions between the early–middle Permian and the Early Triassic, as well as the voluminous late Permian sediment supply, erosion, and/or lack of deposition, indicates a period of tectonic instability (Bourquin et al., 2011). This instability was probably related to an increase and decrease alternation of the basin’s rate of subsidence. This variability at a regional scale could have been related to alternations of rapid,

tectonically controlled subsidence (accompanied by volcanism) with phases of gradual, more extensive thermal subsidence (Bradley, 1982; Ziegler et al., 2001), typical of post-collisional intracratonic basins. At the scale of a single half-graben, the amount of sediment supplied is controlled by the master fault activity relative to the regional uplift and by subsidence rates of the footwall and hangingwall (Doglioni et al., 1998). According to this general picture, we propose that the recycling proxies of the upper Permian and Triassic levels from the Nurra Basin record mainly structural changes that enhanced the subsidence in some basins relative to others or, in the same half-graben, uplifted the footwall with respect to the rapidly subsiding hangingwall, forming morphological steps at

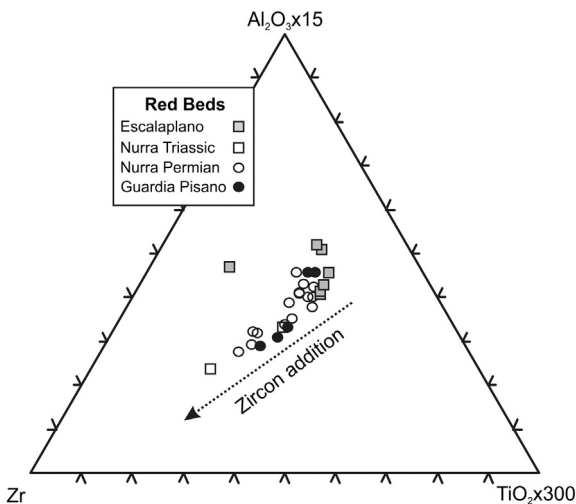


Fig. 13. $15Al_2O_3$ – $300TiO_2$ –Zr ternary plot showing possible sorting effects for Guardia Pisano and Nurra red beds. See text for further details.

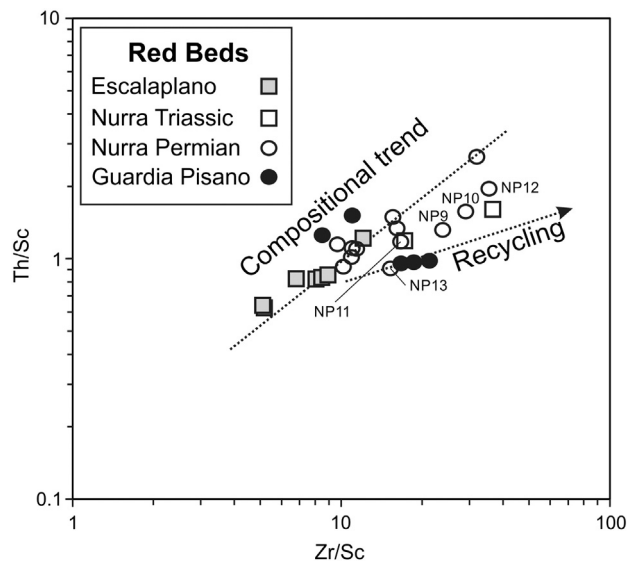


Fig. 14. Th/Sc vs. Zr/Sc plot. Samples depart from the compositional trend indicating zircon addition suggestive of a recycling effect.

the surface and generating erosion and transportation of continental sediments of previous sedimentary cycles. A similar mechanism may also be supposed for the Guardia Pisano Basin (Fig. 12).

More generally, the importance of tectonic setting in controlling mudrock chemistry is well known, as is the existence of a dynamic relationship between the tectonic evolution of a continental block and the composition of its sedimentary mantle (Cox et al., 1995). This relationship can be monitored using the index of compositional variability (ICV = $[(\text{Fe}_2\text{O}_3 + \text{K}_2\text{O} + \text{Na}_2\text{O} + \text{CaO}^* + \text{MgO}^* + \text{TiO}_2)/\text{Al}_2\text{O}_3]$; Cox and Lowe, 1995), which enables estimates of the amount of primary minerals relative to weathered minerals. In this index, CaO^* and MgO^* , excluding the Ca and Mg sources related to the carbonate component, enables estimates of the siliciclastic component only. The ICV value is highest for detrital ferromagnesian minerals and feldspars, and lowest for authigenic minerals that form during weathering. Thus, ICV values for siltstones and shales with relatively abundant primary detrital minerals should be greater than 1. In contrast, siltstones and shales composed of abundant secondary minerals have an ICV value less than 1, as a consequence of more intense weathering and negligible tectonic uplift (Cox and Lowe, 1995). In the Guardia Pisano Basin, the ICV values are generally above 1 (average ICV = 1.14 ± 0.18) and show an increase in the uppermost levels GPP3, GPP4, and GPP5, which are distributed along a recycling trend.

In the Nurra Basin, although there is some degree of uncertainty due to K addition during diagenesis, there is a trend towards ICV values above 1 for the uppermost Permian and the two Triassic levels, which are those levels affected by recycling. Contrasting results are observed for the Escalaplano Basin, where ICV values are always above 1, whereas in the Al_2O_3 – TiO_2 –Zr diagram, the Th/Sc and the Th/Zr ratios exclude any recycling influence. We surmise that the ICV values in the Escalaplano Basin samples are clearly affected by unrealistically high values of CaO^* and MgO^* , even though corrections were made based on the mineralogical abundances of carbonate minerals. This indicates that the ICV proxy must be used with care in carbonate-rich mudrocks.

5.2.3. Palaeoredox changes

Although the sampled levels formed in a homogeneous environment (i.e., an alluvial plain depositional system), changes in the redox conditions during either the depositional or post-depositional stages cannot be excluded. Redox-sensitive trace elements or ratios have often been used to decipher the palaeoredox condition of sediments (e.g., Algeo and Maynard, 2004; Mongelli et al., 2012). The V/Cr ratio has proven to be one of the most useful in this regard (Jones and Manning, 1994); under oxic conditions, V and Cr occur in solution as H_2VO_4 and CrO_4 , whereas under reducing conditions, they are largely insoluble. Jones and Manning (1994) concluded that oxic to highly oxic conditions are associated with $\text{V}/\text{Cr} < 2$, but reducing conditions are associated with $\text{V}/\text{Cr} > 4.25$. In the present case, as expected, V/Cr is ≤ 2 in almost all the samples (Table 3). Minor deviations from these conditions are observed in the basal NP2 ($\text{V}/\text{Cr} = 2.5$) and the uppermost NP13 ($\text{V}/\text{Cr} = 2.6$) Permian levels of the Nurra succession and in the uppermost level (ET7, $\text{V}/\text{Cr} = 3.1$) of the Escalaplano Basin. In samples NP13 and ET7, less oxic conditions are coupled with high CaO and MgO contents related to carbonate abundance, likely involving a decrease of detrital supply under more arid climatic conditions, which in turn favoured partial oxygen consumption during the depositional stage. The barium enrichment observed in NP13, likely recording the presence of authigenic barite, may indicate significant concentration of dissolved SO_4 , as observed in many modern hypersaline environments (Mongelli et al., 2012 and references therein).

5.2.4. Parental affinity

Trace elements, and especially the REEs, Th, and Sc, are useful for constraining the average provenance compositions of mudrocks and siltstones (e.g., Taylor and McLennan, 1985; Fedo et al., 1996; Cullers and Berendsen, 1998; Mongelli, 2004; Perri et al., 2011), including red

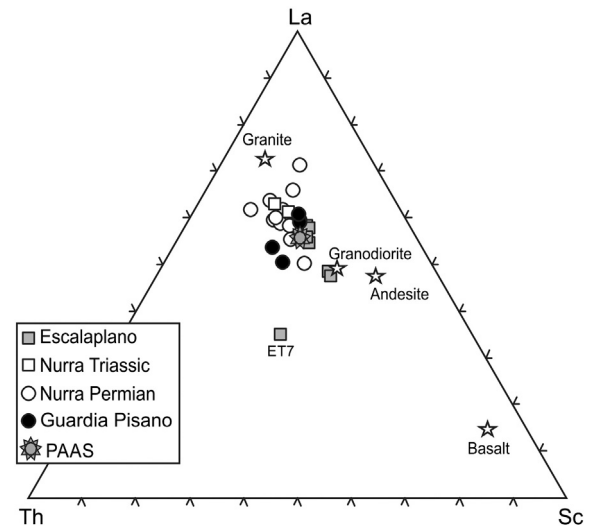


Fig. 15. La-Th-Sc ternary plot. The redbeds fall in a region close to the PAAS point suggesting a negligible mafic supply.

beds of the Tethyan domain (Mongelli et al., 2006; Perrone et al., 2006; Critelli et al., 2008; Zaghloul et al., 2010; Perri et al., 2013). A widely used tool to discriminate sediments derived from felsic sources to progressively more mafic sources is the La-Th-Sc plot (Bhatia and Crook, 1986; Cullers, 1994). The Sardinian siltstones and shales fall in a region close to the PAAS point (Fig. 15), suggesting a provenance from upper continental sources and involving negligible mafic supply. This reflects the paucity of mafic rocks in the Variscan basement and excludes any contribution from the mafic dyke swarms of transitional to alkaline signature, most of which were emplaced during the late Permian to Early Triassic (260–245 Ma; Cocherie et al., 2005; Gaggero et al., 2007). Also, in the $(\text{Gd}/\text{Yb})_N$ versus Eu/Eu^* binary diagram (Fig. 16), most of the samples fall in (or are close to) the field of the post-Archean cratonic sediments (McLennan, 1989). Furthermore, the Eu anomaly, which is the more conservative provenance proxy (McLennan et al., 1993; Mongelli et al., 1998; Cullers, 2000), is for each basin and on the average lower than that of the PAAS, suggesting a more felsic parental affinity. This likely indicates that, in addition to phyllites of the metapelitic complex, the supply from both leucosome in migmatites and early Variscan anatectic peraluminous granitoids (320–310 Ma; Casini et al., 2012) of the Sardinia–Corsica Batholith

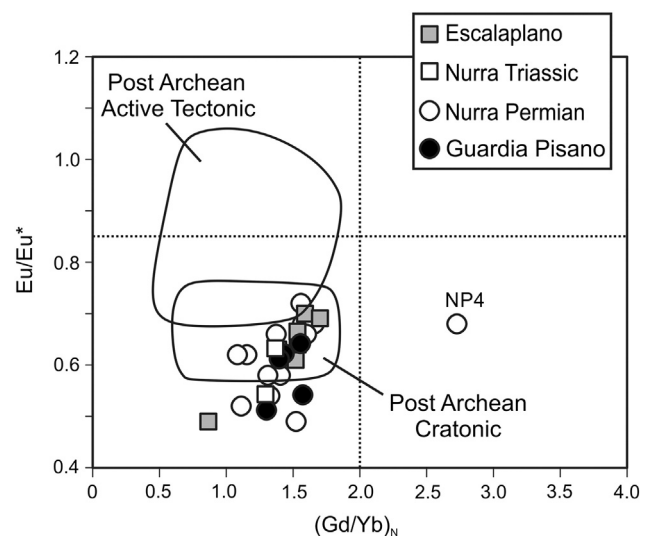


Fig. 16. $(\text{Gd}/\text{Yb})_N$ vs. Eu/Eu^* binary diagram confirming a more felsic parental affinity for Sardinian red beds. See text for further details.

was not negligible. The significant component of lower Permian volcanic rocks of the Nurra succession (in the Porto Ferro and Cala del Vino formations) should be considered and testifies to the increase in the subsidence rate of this basin during the middle–late Permian and the recycling of its relatively uplifted basal portion to the north of the Baratz Fault (Fig. 1).

6. Summary

Measurements of geochemical and mineralogical proxies for the Permian and Triassic sequences of Sardinia studied in this paper have allowed important palaeoenvironmental inferences to be made concerning the early–middle Permian to Early Triassic transition from Pangaea B configuration to Pangaea A at the northern Gondwana margin (Muttoni et al., 2009). This has contributed to the unravelling of the palaeoclimatic conditions related to the South European Variscan Chain during its post-collisional denudation and erosion.

During the late Carboniferous–early Permian, the Variscan relief likely had significant elevation because the axial zone of the chain, in northern Sardinia, was subjected to exhumation rates greater than 1 mm/yr (Cortesogno et al., 1998). This hypothesis agrees with Becq-Giraudon et al. (1996) which proved that during the Carboniferous–Permian transition, the Massif Central in France had an elevation higher than 4500 m. In contrast, in western Pangaea, where the Panthalassa Ocean was forming at the same time, terranes were affected by very low exhumation rates (Eusden and Lux, 1994). As proposed by Fluteau et al. (2001) for other sectors of the South Variscan domain, also in the axial zone of Sardinia, where deep crustal levels were exhumed, high relief may have endured through to the middle Permian, that in the Nurra basin is dated on the basis of the finding of a huge caseid (Ronchi et al., 2011).

The presence of the South European Variscan Chain involved more humid conditions (punctuated by more arid episodes as testified by dolocretes) in the axial zone relative to the foreland, on account of windward-side orographic rainfalls, consistent with the weathering indices calculated for the studied sediments. Furthermore, the palaeoweathering proxy (CIW) for the Nurra Basin samples is also consistent with a change towards a more humid climate at the end of the middle Permian, which produced more intense chemical weathering. Tectonic instability at a regional scale plays also an important role, since it promoted structural changes that allowed sedimentary recycling and subsidence, which in turn caused diagenetic K-metasomatism. The increase in the rate of subsidence in some basins during the middle–late Permian and the recycling of the uplifted basement are also suggested by evaluation of the source-area(s) lithologies, which likely include, in addition to the metapelitic rocks from the green schist facies basement, the migmatitic leucosomes and Early Variscan anatectic granitoids, and the lower Permian volcanic rocks of the Nurra succession.

Acknowledgements

Authors wish to thank two referees (F. Perri and anonymous) for their helpful and constructive comments and suggestions. This work was financially supported by a Banco di Sardegna Foundation grant.

References

- Algeo, T.J., Maynard, J.B., 2004. Trace-element behavior and redox facies in core shales of Upper Pennsylvanian Kansas-type cyclothems. *Chem. Geol.* 206, 289–318.
- Alonso-Zarza, A.M., Zhao, Z., Song, C.H., Li, J.J., Zhang, J., Martin-Perez, A., Martin-Garcia, R., Wang, X.X., Zhang, Y., Zhang, M.H., 2009. Mudflat/distal fan and shallow lake sedimentation (upper Vallesian–Turolian) in the Tianshui Basin, Central China: evidence against the late Miocene eolian loess. *Sediment. Geol.* 222 (1), 42–51.
- Barca, S., Costamagna, L.G., 2006. Stratigrafia, analisi di facies ed architettura deposizionale della successione Permiana di Guardia Pisano (Sulcis, Sardegna SW). *Boll. Soc. Geol. Ital.* 125, 3–19.
- Basilici, G., Dal Bò, P.F.F., Bernardes Ladeira, F.S., 2009. Climate-induced sediment–palaeosol cycles in a Late Cretaceous dry aeolian sand sheet: Marília Formation (North–West Bauru Basin, Brazil). *Sedimentology* 56 (6), 1876–1904.
- Becq-Giraudon, J.F., Montecat, C., Van Den Driessche, J., 1996. Hercynian high-altitude phenomena in the French Massif Central: tectonic implications. *Palaeogeogr. Palaeoclimatol. Palaeoecol.* 122 (14), 227–241.
- Bertoluzza, L., Perotti, C.R., 1997. A finite-element model of the stress field in strike-slip basins: implications for the Permian tectonics of the Southern Alps (Italy). *Tectonophysics* 280 (1–2), 185–197.
- Bhatia, M.R., Crook, K.A.W., 1986. Trace element characteristics of graywackes and tectonic setting discrimination of sedimentary basins. *Contrib. Mineral. Petrol.* 92, 181–193.
- Bourquin, S., Bercovicci, A., López-Gómez, J., Diez, J.B., Broutin, J., Ronchi, A., Durand, M., Arché, A., Linol, B., Amour, F., 2011. The Permian–Triassic transition and the onset of Mesozoic sedimentation at the northwestern peri-Tethyan domain scale: palaeogeographic maps and geodynamic implications. *Palaeogeogr. Palaeoclimatol. Palaeoecol.* 299, 265–280.
- Bourquin, S., Durand, M., Diez, J.B., Broutin, J., Fluteau, F., 2007. The Permian–Triassic boundary and Early Triassic sedimentation in Western European basins: an overview. *J. Iber. Geol.* 33 (2), 221–236.
- Bradley, D.C., 1982. Subsidence in late Paleozoic basins in the northern Appalachians. *Tectonics* 1 (1), 107–123.
- Broutin, J., Cabanis, B., Châteauneuf, J.J., Derooin, J.P., 1994. Évolution biostratigraphique, magmatique et tectonique du domaine paléotéthysien occidental (SW de l'Europe): implications paléogéographiques au Permien inférieur. *Bull. Soc. Geol. Fr.* 165, 163–179.
- Buzzi, L., Gaggero, L., Oggiano, G., 2008. The Santa Giusta ignimbrite (NW Sardinia): a clue for the magmatic, structural and sedimentary evolution of a Variscan segment between Early Permian and Triassic. *Boll. Soc. Geol. Ital.* 127 (3), 683–695.
- Carmignani, L., Carosi, R., Di Pisa, A., Gattiglio, M., Musumeci, G., Oggiano, G., Pertusati, P.C., 1994. The Hercynian chain in Sardinia (Italy). *Geodin. Acta* 7 (1), 31–47.
- Casini, L., Cuccuru, S., Maino, M., Oggiano, G., Tiepolo, M., 2012. Emplacement of the Arzachena Pluton (Corsica–Sardinia Batholith) and the geodynamics of incoming Pangaea. *Tectonophysics* 544, 31–49.
- Casini, L., Oggiano, G., 2008. Late orogenic collapse and thermal doming in the northern Gondwana margin incorporated in the Variscan Chain: a case study from the Ozieri Metamorphic Complex, northern Sardinia, Italy. *Gondwana Res.* 13 (3), 396–406.
- Cassinis, G., Durand, M., Ronchi, A., 2003. Permian–Triassic continental sequences of Northwest Sardinia and South Provence: stratigraphic correlations and palaeogeographical implications. *Boll. Soc. Geol. Ital. (Spec. Vol.)* 2, 119–129.
- Cavalcante, F., Fiore, S., Lettino, A., Piccarreta, G., Tateo, F., 2007. Illite–smectite mixed layers in sicilide shales and piggy-back deposits of the Gorgoglione Formation (Southern Apennines): geological inferences. *Boll. Soc. Geol. Ital. (Ital. J. Geosci.)* 126 (2), 241–254.
- Chen, B., Joachimski, M.M., Shen, S., Lambert, L.L., Lai, X., Wang, X., Chen, X., Yuan, D., 2013. Permian ice volume and palaeoclimate history: oxygen isotope proxies revisited. *Gondwana Res.* 24 (1), 77–89.
- Cocherie, A., Rossi, P., Fanning, C.M., Guerrot, C., 2005. Comparative use of TIMS and SHRIMP for U–Pb zircon dating of A-type granites and mafic tholeiitic layered complexes and dykes from the Corsican Batholith (France). *Lithos* 82, 185–219.
- Conti, P., Carmignani, L., Oggiano, G., Funedda, A., Cerbai, N., Eltrudis, A., 1999. From thickening to extension in the Variscan belt—kinematic evidence from Sardinia (Italy). *Terra Nova* 11 (2–3), 93–99.
- Cortesogno, L., Cassinis, G., Dallagiovanna, G., Gaggero, L., Oggiano, G., Ronchi, A., Seno, S., Vanossi, M., 1998. The Variscan post-collisional volcanism in Late Carboniferous–Permian sequences of Ligurian Alps, Southern Alps and Sardinia (Italy): a synthesis. *Lithos* 45 (1–4), 305–328.
- Cortesogno, L., Gaggero, L., Oggiano, G., Paquette, J.L., 2004. Different tectono-thermal evolutionary paths in eclogitic rocks from the axial zone of the Variscan chain in Sardinia (Italy) compared with the Ligurian Alps. *Ofioliti* 29, 125–144.
- Costamagna, L.G., Barca, S., Del Rio, M., Pittau, P., 2000. Stratigrafia, palaeogeografia ed analisi di facies deposizionale del Trias del Sarcidano-Gerrei (Sardegna SE). *Boll. Soc. Geol. Ital.* 119, 437–496.
- Cox, R., Lowe, D.R., 1995. Controls on sediment composition on a regional scale. *Conceptual view.* *J. Sediment. Res.* 65, 1–12.
- Cox, R., Lowe, D.R., Cullers, R.L., 1995. The Influence of sediment recycling and basement composition on evolution of mudrock chemistry in Southwestern United States. *Geochim. Cosmochim. Acta* 59, 2919–2940.
- Critelli, S., Mongelli, G., Perri, F., Martín-Algarra, A., Martín-Martín, M., Perrone, V., Dominici, R., Sonnino, M., Zaghoul, M.N., 2008. Compositional and geochemical signatures for the sedimentary evolution of the Middle Triassic–Lower Jurassic continental redbeds from Western-Central Mediterranean Alpine Chains. *J. Geol.* 116, 375–386.
- Cruciani, G., Dini, A., Franceschelli, M., Puxeddu, M., Utzeri, D., 2010. Metabasite from the Variscan belt in NE Sardinia, Italy: within-plate OIB-like melts with very high Sr and low Nd isotope ratios. *Eur. J. Mineral.* 22 (4), 509–523.
- Cullers, R.L., 1994. The controls on the major and trace element variation of shales, siltstones, and sandstones of Pennsylvanian–Permian age from uplifted continental blocks in Colorado to platform sediments in Kansas, USA. *Geochim. Cosmochim. Acta* 58, 4955–4972.
- Cullers, R.L., 2000. The geochemistry of shales, siltstones and sandstones of Pennsylvanian–Permian age, Colorado, USA: implications for provenance and metamorphic studies. *Lithos* 51, 181–203.
- Cullers, R.L., Berendsen, P., 1998. The provenance and chemical variation of sandstones associated with the Mid-continent Rift System, U.S.A. *Eur. J. Mineral.* 10, 987–1002.

- De la Horra, R., Benito, M.I., López-Gómez, J., Arché, A., Barrenechea, J.F., Luque, J., 2008. Palaeoenvironmental significance of Late Permian palaeosols in the South-Eastern Iberian Ranges, Spain. *Sedimentology* 55, 1849–1873.
- De la Horra, R., Galan-Abellan, A.B., Lopez-Gomez, J., Sheldon, N.D., Barrenechea, J.F., Luque, J., Arché, A., Benito, M.I., 2012. Paleocological and paleoenvironmental changes during the continental Middle–Late Permian transition at the SE Iberian Ranges, Spain. *Global Planet. Change* 94–95, 46–61.
- Diez, J.B., Broutin, J., Ferrer, J., 2005. Difficulties encountered in defining the Permian–Triassic boundary in Buntsandstein facies of the western Peritethyan domain based on palynological data. *Palaeogeogr. Palaeoclimatol. Palaeoecol.* 229, 40–53.
- Dogliani, C., Dagostino, N., Mariotti, G., 1998. Normal faulting vs regional subsidence and sedimentation rate. *Mar. Pet. Geol.* 15 (8), 737–750.
- Durand, M., 2008. Permian to Triassic continental successions in southern Provence (France): an overview. *Boll. Soc. Geol. Ital.* 127 (3), 697–716.
- Eusden Jr., J.D., Lux, D.R., 1994. Slow late Paleozoic exhumation in the Presidential Range of New Hampshire as determined by the 40Ar/39Ar relief method. *Geology* 22 (10), 909–912.
- Evensen, N.M., Hamilton, P.J., O’Nions, R.K., 1978. Rare earth abundances in chondritic meteorites. *Geochim. Cosmochim. Acta* 42, 1199–1212.
- Fedo, C.M., Eriksson, K.A., Krogstad, E.J., 1996. Geochemistry of shales from the Archean (≈ 3.0 Ga) Buhwa Greenstone belt, Zimbabwe: implication for provenance and source area weathering. *Geochim. Cosmochim. Acta* 60, 1751–1763.
- Fluteau, F., Besse, J., Broutin, J., Ramstein, G., 2001. The Late Permian climate. What can be inferred from climate modelling concerning Pangea scenarios and Hercynian range altitude? *Palaeogeogr. Palaeoclimatol. Palaeoecol.* 167 (1–2), 39–71.
- Fontana, D., Neri, C., Ronchi, A., Stefani, C., 2001. Stratigraphic architecture and composition of the Permian and Triassic siliclastic succession of Nurra (northwestern Sardinia). In: Cassinis, G. (Ed.), *Permian Continental Deposits of Europe and other areas. Regional reports and correlations. Proc. Intern. Field Conf. on «The continental Permian of the Southern Alps and Sardinia (Italy). Regional reports and general correlations», 15–25 Sept. 1999, Brescia, Italy. «Natura Bresciana»*. Ann. Mus. Civ. Sc. Nat., Brescia (Italy), Monografia, 25, pp. 149–161.
- Franceschelli, M., Puxeddu, M., Cruciani, G., Utzeri, D., 2007. Metabasites with eclogite facies relics from Variscides in Sardinia, Italy: a review. *Int. J. Earth Sci.* 96 (5), 795–815.
- Funedda, A., 2009. Foreland- and hinterland-verging structures in fold-and-thrust belt: an example from the Variscan foreland of Sardinia. *Int. J. Earth Sci.* 98 (7), 1625–1642.
- Gaggero, L., Oggiano, G., Buzzi, L., Slejko, F., Cortesogno, L., 2007. Post-variscan mafic dikes from the late orogenic collapse to the Tethyan rift: evidence from Sardinia. *Ophioliti* 32 (1), 15–37.
- García, D., Coelho, J., Perrin, M., 1991. Fractionation between TiO₂ and Zr as a measure of sorting within shale and sandstone series (northern Portugal). *Eur. J. Mineral.* 3, 401–414.
- Gómez-Gras, D., Alonso-Zarza, A.M., 2003. Reworked calcretes: their significance in the reconstruction of alluvial sequences (Permian and Triassic, Minorca, Balearic Islands, Spain). *Sediment. Geol.* 158, 299–319.
- Harnois, L., 1988. The CIW index: a new chemical index of weathering. *Sediment. Geol.* 55, 319–322.
- Hassan, S., Ishiga, H., Roser, B.P., Dozen, K., Naka, T., 1999. Geochemistry of Permian–Triassic shales in the Salt Range, Pakistan: implications for provenance and tectonism at the Gondwana margin. *Chem. Geol.* 158, 293–314.
- Isozaki, Y., Aljinovic, D., Kawahata, H., 2011. The Guadalupian (Permian) Kamura event in European Tethys. *Palaeogeogr. Palaeoclimatol. Palaeoecol.* 308, 12–21.
- Jones, B., Manning, D.A.C., 1994. Comparison of geochemical indices used for the interpretation of palaeoredox conditions in ancient mudstones. *Chem. Geol.* 111, 111–129.
- Kossovaya, O.L., 2009. Artinskian–Wordian antitropical rugose coral associations: a palaeogeographical approach. *Palaeoworld* 18, 136–151.
- Laviano, R., 1987. Analisi mineralogica quantitativa di argille mediante diffrattometria di raggi X, in *Procedura di analisi di materiali argillosi. Atti del workshop del Centro Ricerche Energia Ambiente, Roma, Ente Nazionale Energie Alternative (ENEA)* 215–234.
- Lindgreen, H., Surllyk, F., 2000. Upper Permian–Lower Cretaceous clay mineralogy of East Greenland: provenance, palaeoclimate and vulcanicity. *Clay Miner.* 35, 791–806.
- Linol, B., Bercovici, A., Bourquin, S., Diez, J.B., Lopez-Gomez, J., Broutin, J., Durand, M., Villanueva-Amadoz, U., 2009. Late Permian to Middle Triassic correlations and palaeogeographical reconstructions in south-western European basins: new sedimentological data from Minorca (Balearic Islands, Spain). *Sediment. Geol.* 220 (1–2), 77–94.
- Lynn, W.C., Tu, H.Y., Franzmeier, D.P., 1971. Authigenic barite in soils. *Soil Sci. Soc. Am. J.* 35, 160–161.
- López-Gómez, J., Arche, A., Marzo, M., Durand, M., 2005. Stratigraphical and palaeogeographical significance of the continental sedimentary transition across the Permian–Triassic boundary in Spain. *Palaeogeogr. Palaeoclimatol. Palaeoecol.* 229, 3–23.
- López-Gómez, J., Galan-Abellan, B., de la Horra, R., Barrenechea, J.F., Arche, A., Bourquin, S., Marzo, M., Durand, M., 2012. Sedimentary evolution of the continental Early–Middle Triassic Canizar Formation (Central Spain): implications for life recovery after the Permian–Triassic crisis. *Sediment. Geol.* 249, 26–44.
- McLennan, S.M., 1989. Rare earth elements in sedimentary rocks: influence of provenance and sedimentary processes. In: Lipin, B.R., McKay, G.A. (Eds.), *Geochemistry and Mineralogy of Rare Earth Elements*. Min. Soc. Am. Rev. Mineral., 21, pp. 169–200.
- McLennan, S.M., Hemming, D.K., Hanson, G.N., 1993. Geochemical approaches to sedimentation, provenance and tectonics. *Geol. Soc. Am. Spec. Pap.* 284, 284, 21–284, 40.
- Mikhailova, E.A., Post, C.J., 2006. Organic carbon stocks in the Russian Chernozem. *Eur. J. Soil Sci.* 57, 330–336.
- Mongelli, G., 2004. Rare-earth elements in Oligo-Miocene pelitic sediments from Lagonegro basin, southern Apennines, Italy: implications for provenance and source-area weathering. *Int. J. Earth Sci.* 93, 612–620.
- Mongelli, G., Critelli, S., Perri, F., Sonnino, M., Perrone, V., 2006. Sedimentary recycling, provenance and paleoweathering from chemistry and mineralogy of Mesozoic continental redbed mudrocks, Peloritani mountains, southern Italy. *Geochem. J.* 40, 197–209.
- Mongelli, G., Cullers, R.L., Dinelli, E., Rottura, A., 1998. Elemental mobility during the weathering of exposed lower crust: the kinzigitic paragneisses from the Serre, Calabria, southern Italy. *Terra Nova* 10 (4), 190–195.
- Mongelli, G., Marni, P., Oggiano, G., Sinisi, R., 2012. Messinian palaeoclimate and palaeoenvironment in the western Mediterranean realm: insights from the geochemistry of continental deposits of NW Sardinia (Italy). *Int. Geol. Rev.* 54, 971–990.
- Muttoni, G., Gaetani, M., Kent, D.V., Sciunnach, D., Angiolini, L., Berra, F., Garzanti, E., Mattei, M., Zanchi, A., 2009. Opening of the Neo-Tethys Ocean and the Pangea B to Pangea A transformation during the Permian. *GeoArabia* 14 (4), 17–48.
- Nesbitt, H.W., Young, G.M., 1982. Early Proterozoic climates and plate motions inferred from major element chemistry of lutites. *Nature* 299, 715–717.
- Nesbitt, H.W., Young, G.M., 1984. Prediction of some weathering trends of plutonic and volcanic rocks based on thermodynamic and kinetic considerations. *Geochim. Cosmochim. Acta* 48, 1523–1534.
- Nesbitt, H.W., Young, G.M., 1989. Formation and diagenesis of weathering profiles. *J. Geol.* 97, 129–147.
- Oggiano, G., Gaggero, L., Funedda, A., Buzzi, L., Tiepolo, M., 2010. Multiple early Paleozoic volcanic events at the northern Gondwana margin: U–Pb age evidence from the Southern Variscan branch (Sardinia, Italy). *Gondwana Res.* 17 (1), 44–58.
- Pecorini, G., 1974. Nuove osservazioni sul Permo-Triass di Escalaplano (Sardegna sud-orientale). *Boll. Soc. Geol. Ital.* 93, 991–999.
- Perri, F., Critelli, S., Cavalcante, F., Mongelli, G., Dominici, R., Sonnino, M., De Rosa, R., 2012. Provenance signatures for the Miocene volcanoclastic succession of the Tufti di Tusa Formation, southern Apennines, Italy. *Geol. Mag.* 149, 423–442.
- Perri, F., Critelli, S., Martín-Algarra, A., Martín-Martín, M., Perrone, V., Mongelli, G., Zattin, M., 2013. Triassic redbeds in the Malaguide Complex (Betic Cordillera–Spain): petrography, geochemistry and geodynamic implications. *Earth Sci. Rev.* 117, 1–28.
- Perri, F., Critelli, S., Mongelli, G., Cullers, R.L., 2011. Sedimentary evolution of the Mesozoic continental redbeds using geochemical and mineralogical tools: the case of Upper Triassic to Lowermost Jurassic Monte di Gioiosa mudrocks (Sicily, southern Italy). *Int. J. Earth Sci.* 100 (7), 1569–1587.
- Perrone, V., Martín-Algarra, A., Critelli, S., Decandia, F.A., D’Errico, M., Estevez, A., Iannace, A., Lazzarotto, A., Martín-Martín, M., Martín-Rojas, I., Mazzoli, S., Messina, A., Mongelli, G., Vitale, S., Zaghoul, M.N., 2006. “Verrucano” and “Pseudoverrucano” in the central-western Mediterranean Alpine chains: palaeogeographic evolution and geodynamic significance. In: Chalouan, A., Moratti, G. (Eds.), *Geology and Active Tectonics of the Western Mediterranean Region and North Africa*. Geological Society (London), Special Publication, 262, pp. 1–46.
- Pittau, P., 2002. Palynofloral biostratigraphy of the Permian and Triassic sequences of Sardinia. *Rend. Soc. Paleontol. Ital.* 1, 93–109.
- Plank, T., Langmuir, C.H., 1998. The chemical composition of subducting sediment and its composition for the crust and mantle. *Chem. Geol.* 145, 325–394.
- Podwojewski, P., 1995. The occurrence and interpretation of carbonate and sulfate minerals in a sequence of Vertisols in New Caledonia. *Geoderma* 65, 223–248.
- Retallack, G.J., 1997. *A Colour Guide to Paleosols*. John Wiley and Sons, Chichester (175 pp.).
- Retallack, G.J., 2001. *Scoyenia burrows from Ordovician palaeosols of the Juniata Formation in Pennsylvania*. *Palaentology* 44 (2), 209–235.
- Retallack, G.J., 2013. Permian and Triassic greenhouse crises. *Gondwana Res.* 24 (1), 90–103.
- Ronchi, A., Sacchi, E., Romano, M., Nicosia, U., 2011. A huge caseid pelycosaur from north-western Sardinia and its bearing on European Permian stratigraphy and palaeobiogeography. *Acta Palaentol. Pol.* 56 (4), 723–738.
- Ronchi, A., Sarria, E., Broutin, J., 2008. The “Autuniano Sardo”: basic features for a correlation through the Western Mediterranean and Paleoeurope. *Boll. Soc. Geol. Ital. (Ital. J. Geosci.)* 127 (3), 655–681.
- Roscher, M., Schneider, J.W., 2006. Permo–Carboniferous climate: Early Pennsylvanian to Late Permian climate development of Central Europe in a regional and global context. *Geol. Soc. Spec. Pub.* 265, 95–136.
- Rossi, P., Oggiano, G., Cocherie, A., 2009. A restored section of the “southern Variscan realm” across the Corsica–Sardinia microcontinent. *C. R. Geosci.* 341, 224–238.
- Roy, D.K., Roser, B.P., 2013. Climatic control on the composition of Carboniferous–Permian Gondwana sediments, Khalaspir basin, Bangladesh. *Gondwana Res.* 23 (3), 1163–1171.
- Sheldon, N.D., 2005. Do red beds indicate paleoclimatic conditions? A Permian case study. *Palaeogeogr. Palaeoclimatol. Palaeoecol.* 228 (3–4), 305–319.
- Sheldon, N.D., Tabor, N.J., 2009. Quantitative paleoenvironmental and paleoclimatic reconstruction using paleosols. *Earth Sci. Rev.* 95, 1–52.
- Shen, S.Z., 2013. Late Paleozoic deep Gondwana and its peripheries: stratigraphy, biological events, paleoclimate and paleogeography. *Gondwana Res.* 24 (1), 1–4.
- Sobecki, T.M., Wilding, L.P., 1983. Formation of calcic and argillic horizons in selected soils of the Texas Coast Prairie. *Soil Sci. Soc. Am. J.* 47, 707–715.
- Stoops, G.J., Zavaleta, A., 1978. Micromorphological evidence of barite neof ormation in soils. *Geoderma* 20, 63–70.
- Takeo, N., 2005. Atlas of Eh–pH diagrams. Intercomparison of thermodynamic databases. *Geol. Surv. Jpn* 419, 287.
- Taylor, S.R., McLennan, S.M., 1985. *The Continental Crust: Its Composition and Evolution*. Blackwell, Oxford.

- van Wees, J.D., Stephenson, R.A., Ziegler, P.A., Bayer, U., McCann, T., Dadlez, R., Gaupp, R., Narkiewicz, M., Bitzer, F., Scheck, M., 2000. On the origin of the Southern Permian Basin, Central Europe. *Mar. Pet. Geol.* 17 (1), 43–59.
- von Raumer, J.F., Stampfli, G.A., Bussy, F., 2003. Gondwana-derived microcontinents—the constituents of the Variscan and Alpine collisional orogens. *Tectonophysics* 365 (1–4), 7–22.
- Zaghloul, M.N., Critelli, S., Perri, F., Mongelli, G., Perrone, V., Sonnino, M., Tucker, M., Aiello, M., Ventimiglia, C., 2010. Depositional systems, composition and geochemistry of Triassic rifted-continental margin redbeds of the Internal Rif Chain, Morocco. *Sedimentology* 57, 312–350.
- Zeh, A., Cosca, M.A., Bratz, H., Okrusch, M., Tichomirowa, M., 2000. Simultaneous horst-basin formation and magmatism during Late Variscan transtension: evidence from Ar-40/Ar-39 and Pb-207/Pb-206 geochronology in the Ruhla Crystalline Complex. *Int. J. Earth Sci.* 89 (1), 52–71.
- Ziegler, P.A., Cloetingh, S., Guiraud, R., Stampfli, G.M., 2001. Peri-Tethyan platforms: constraints on dynamics of rifting and basin inversion. In: Ziegler, P.A., Cavazza, W., Robertson, A.H.F., Crasquin-Soleau, S. (Eds.), *Peri-Tethys Mem. 6: Peri-Tethyan Rift/Wrench Basins and Passive Margins*. Mém. Mus. Natn. Hist. Nat., Paris, 186, pp. 9–49.